KEK-TH-1203, FERMILAB-PUB-07-651-T
CERN-PH-TH/2007-258, MAN/HEP/2007/43
ANL-HEP-PR-07-105, EFI-07-38
December 2007

CPsuperH2.0:
an Improved Computational Tool for Higgs Phenomenology in the MSSM with Explicit CP Violation

J. S. Lee[a,b], M. Carena[c], J. Ellis[d], A. Pilaftsis[e] and C. E. M. Wagner[f,g]

[a] *Theory Group, KEK, Oho 1-1 Tsukuba, 305-0801, Japan*

[b] *Department of Physics, National Central University, Chung-Li, Taiwan 32054*

[c] *Fermilab, P.O. Box 500, Batavia IL 60510, U.S.A.*

[d] *Theory Division, CERN, CH-1211 Geneva 23, Switzerland*

[e] *School of Physics and Astronomy, University of Manchester, Manchester M13 9PL, United Kingdom*

[f] *HEP Division, Argonne National Laboratory, 9700 Cass Ave., Argonne, IL 60439, USA*

[g] *Enrico Fermi Institute, Univ. of Chicago, 5640 Ellis Ave., Chicago, IL 60637, USA*

ABSTRACT

We describe the Fortran code `CPsuperH2.0`, which contains several improvements and extensions of its predecessor `CPsuperH`. It implements improved calculations of the Higgs-boson pole masses, notably a full treatment of the 4×4 neutral Higgs propagator matrix including the Goldstone boson and a more complete treatment of threshold effects in self-energies and Yukawa couplings, improved treatments of two-body Higgs decays, some important three-body decays, and two-loop Higgs-mediated contributions to electric dipole moments. `CPsuperH2.0` also implements an integrated treatment of several B-meson observables, including the branching ratios of $B_s \to \mu^+\mu^-$, $B_d \to \tau^+\tau^-$, $B_u \to \tau\nu$, $B \to X_s\gamma$ and the latter's CP-violating asymmetry $\mathcal{A}_{\rm CP}$, and the supersymmetric contributions to the $B^0_{s,d} - \bar{B}^0_{s,d}$ mass differences. These additions make `CPsuperH2.0` an attractive integrated tool for analyzing supersymmetric CP and flavour physics as well as searches for new physics at high-energy colliders such as the Tevatron, LHC and linear colliders. *

*The program may be obtained from `http://www.hep.man.ac.uk/u/jslee/CPsuperH.html`.

1 Introduction

With the imminent advent of the LHC, particle physics experiments are poised to explore the TeV energy range directly for the first time. There are several reasons to expect new physics in this energy range, such as the origin of particle masses and electroweak symmetry breaking, the hierarchy problem and the nature of dark matter. In parallel with the direct exploration of the TeV scale, precision experiments at low energies continue to place important constraints on the possible flavour and CP-violating structure of any TeV-scale physics. Prominent examples include experiments on B and K mesons, and probes of electric dipole moments [1]. It is clearly desirable to develop computational tools that can be used to calculate consistently observables for both low- and high-energy experiments in a coherent numerical framework. This is particularly desirable in view of the possibility that the dominance of matter over antimatter in the Universe may be due to CP-violating interactions at the TeV scale [2].

Supersymmetry is one of the most prominent possibilities for new TeV-scale physics, and the minimal supersymmetric extension of the Standard Model (MSSM) provides a natural cold dark matter candidate as well as stabilizing the electroweak scale and facilitating the unification of the fundamental interactions. There are many computational tools available for calculations within the MSSM. The first to include CP-violating phases was `CPsuperH` [3], which has been followed by recent versions of `FeynHiggs` [4].

Some of us have recently published an analysis of several B-physics observables taking into account the most general set of CP-violating parameters allowed under the assumption of minimal flavour violation in the supersymmetric sector [5]. For this purpose we used an updated and extended computational tool, `CPsuperH2.0`, which we introduce and describe in this paper.

The main new features of `CPsuperH2.0` are its inclusion of a number of B observables, including the branching ratios of $B_s \to \mu^+\mu^-$, $B_d \to \tau^+\tau^-$, $B_u \to \tau\nu$, $B \to X_s\gamma$ and the latter's CP-violating asymmetry $\mathcal{A}_{\rm CP}$, and the supersymmetric contributions to the $B^0_{s,d} - \bar{B}^0_{s,d}$ mass differences. In addition, `CPsuperH2.0` includes a more complete treatment of Higgs-boson pole masses, based on a full treatment of the 4×4 neutral Higgs propagator matrix including the Goldstone boson and a more complete treatment of threshold effects in self-energies and Yukawa couplings. It also includes improved treatments of two-body Higgs decays, some important three-body decays, and two-loop Higgs-mediated contributions to electric dipole moments. Therefore, `CPsuperH2.0` provides an essentially complete, self-contained and consistent computational tool for evaluating flavour and CP-violating physics at energies up to the TeV scale.

The structure of this paper is as follows. Several updated features of `CPsuperH2.0` are described in Section 2. In particular, in Subsection 2.1 we introduce the improved treatment of Higgs-boson pole masses, and Section 2.2 contains a description of the improvements in the treatment of Higgs decay modes. Then, in Section 3 we describe the `CPsuperH2.0` treatment of two-loop Higgs effects on electric dipole moments. The most important new features are described in Section 4, where we discuss its treatment of B observables. In each Section, we illustrate in figures some typical results obtained using `CPsuperH2.0`.

2 Updated Features of `CPsuperH2.0`

It is to be understood that, throughout this paper, we follow the notations and conventions defined and adopted in `CPsuperH` for the mixing matrices of neutral Higgs bosons, charginos, neutralinos and third–generation sfermions, as well as their masses and couplings, etc. The updates to the original version of `CPsuperH` [3] that are presented here reflect, in part, feedback from users, as well as extending it to B observables.

New common blocks `/HC_RAUX/` and `/HC_CAUX/` have been introduced for the general purpose of storing new numerical outputs which are available in `CPsuperH2.0`:

- `COMMON /HC_RAUX/ RAUX_H`
- `COMMON /HC_CAUX/ CAUX_H`

The two arrays `RAUX_H` and `CAUX_H` are `NAUX`=999 dimensional and only parts of them are being used presently as shown in Tables 1 and 2. The contents of these two new arrays are explained in the corresponding following subsections. These common blocks can also be used by users for their specific purposes.

2.1 Improved Treatment of Higgs-Boson Masses and Propagators

In `CPsuperH2.0` we make three main improvements in the calculation of the Higgs-boson pole masses.

- The finite threshold corrections induced by the exchanges of gluinos and charginos have been included in the top- and bottom-quark self-energies of the neutral and charged Higgs bosons. For the explicit expressions of the self-energies, we refer to Eqs. (B.14), (B.15), and (B.16) of Ref. [6] †.
- Also included are the threshold corrections to the Yukawa couplings $|h_{t,b}|$ in the one-loop running quartic couplings, $\lambda_i^{(1)}(Q = m_t^{\rm pole})$ with $i = 1 - 4$. For the explicit expressions of $\lambda_i^{(1)}$, we refer to Eqs. (3.3)-(3.6) of Ref. [7].

†We find that overall minus signs are missing in the expressions of $\Pi^{P,(c)}_{11,22}(s)$.

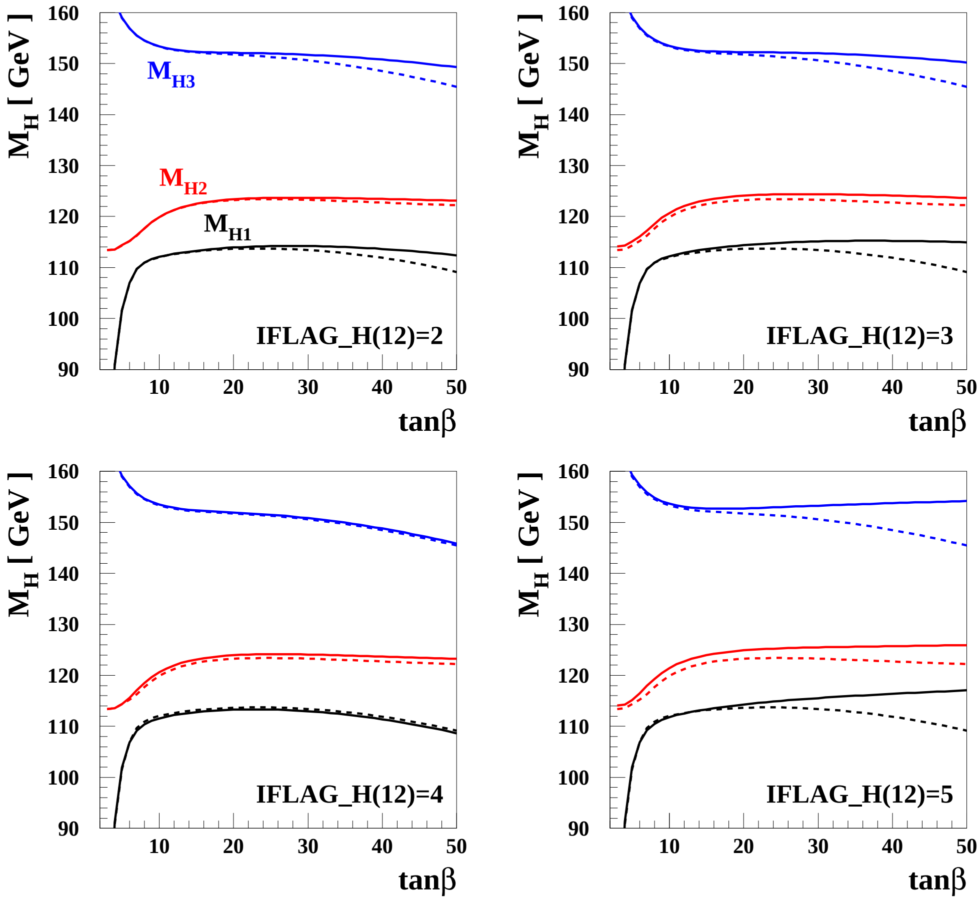

Figure 1: *The masses of the neutral Higgs bosons as functions of* $\tan\beta$ *for the CPX scenario [8] taking* $\Phi_3 = \Phi_{A_{t,b,\tau}} = 90^\circ$ *in the convention* $\Phi_\mu = 0$, $M_{\rm SUSY} = 0.5$ *TeV, and the charged Higgs-boson pole mass* $M_{H^\pm} = 160$ *GeV. In each frame, the dashed line is for the case* `IFLAG_H(12)`$= 1$ *and the solid line for other case indicated.*

- An improved iterative method has been employed for the calculation of the pole masses.

As a help in assessing the improvements in the calculation of Higgs sector, new flags `IFLAG_H(12)` and `IFLAG_H(60)` have been introduced as follows:

- `IFLAG_H(12)`:
  - `IFLAG_H(12)`$= 1$: Gives the same result as that obtained by the older version of `CPsuperH`.
  - `IFLAG_H(12)`$= 2$: Includes only the threshold corrections to the neutral and charged Higgs-boson quark self-energies.

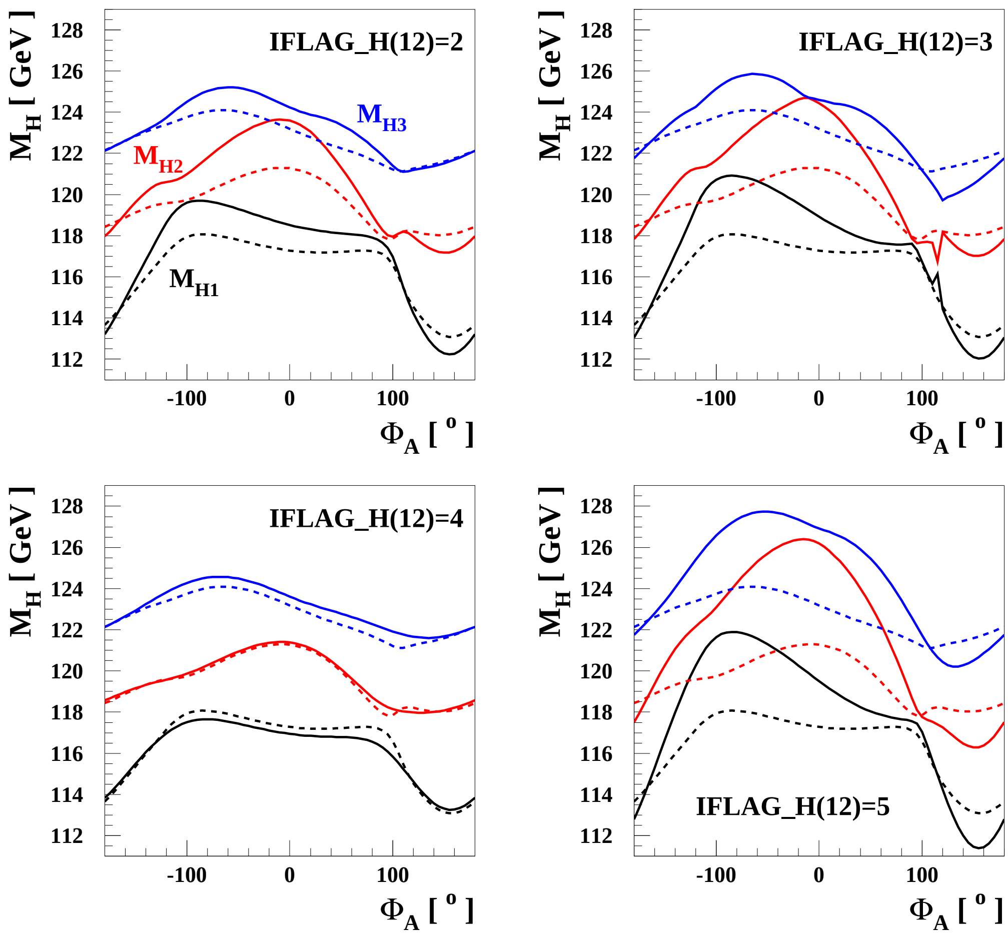

Figure 2: *The masses of the neutral Higgs bosons as functions of the common phase* Φ_A *for the trimixing scenario [9] taking* $\Phi_3 = -90^\circ$*. Specifically, in this scenario,* $\tan\beta = 50$ *and* $M_{H^\pm} = 155$ *GeV. The lines are the same as in Fig. 1.*

- `IFLAG_H(12)`$=3$: Includes only the threshold corrections to $\lambda_i^{(1)}$.
- `IFLAG_H(12)`$=4$: Includes only the iterative method for the pole masses.
- `IFLAG_H(12)`$=5$ or 0: All the improvements are fully included.

• `IFLAG_H(60)`$=1$: This is an error message that appears when the iterative method for the pole masses fails.

The improvement in the threshold corrections to the top- and bottom-quark Yukawa couplings is important when $\tan\beta$ is large and the charged Higgs boson is light. In Figs. 1 and 2, we show the pole masses of the neutral Higgs bosons for the CPX [8] and trimixing [9] scenarios, respectively, when `IFLAG_H(12)` = 2-5 as indicated. In each frame, the old calculation with `IFLAG_H(12)`= 1 (dashed line) is also shown for comparison.

Finally, `RAUX_H(1-6)`, `RAUX_H(10-36)`, and `CAUX_H(1-2)` are allocated for numerical information on the Higgs-sector calculation based on a renormalization-group-improved diagrammatic approach including dominant higher-order logarithmic and threshold corrections [6, 7], see Tables 1 and 2.

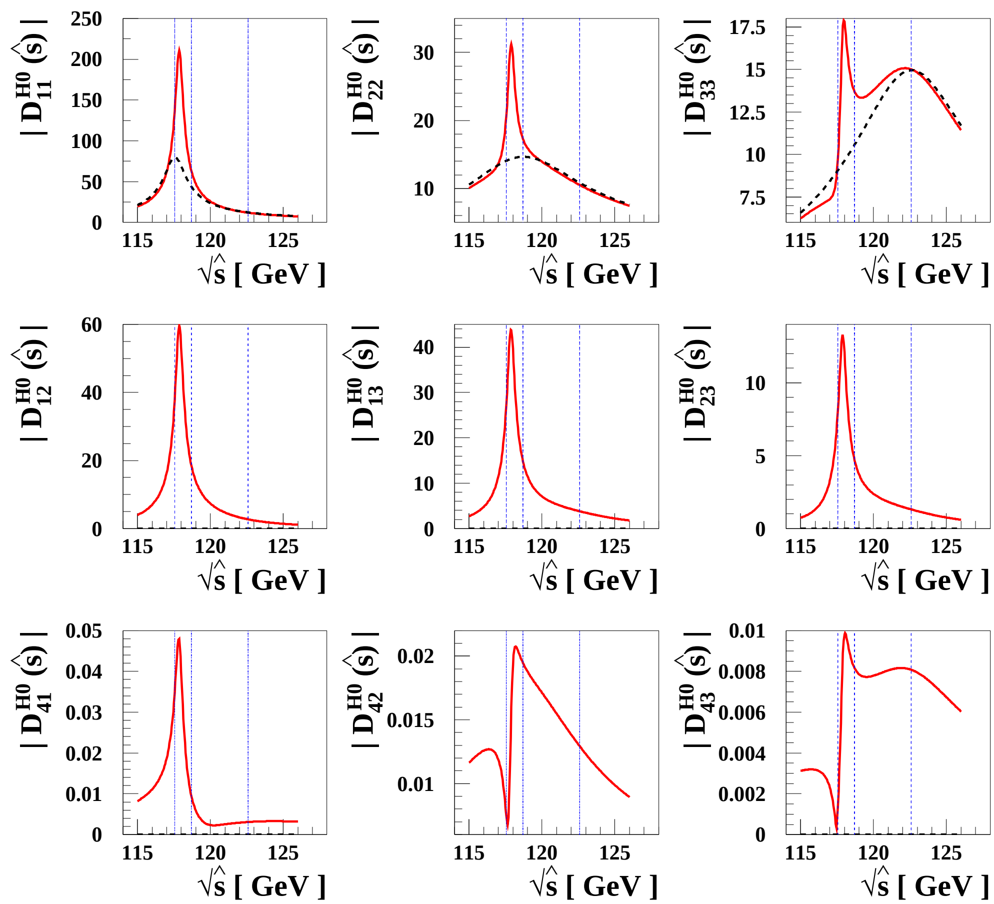

Figure 3: *The absolute value of each component of the neutral Higgs-boson propagator matrix $D^{H^0}(\hat{s})$ with (red solid lines) and without (black dashed lines) including off-diagonal absorptive parts in the trimixing scenario with $\Phi_A = -\Phi_3 = 90^\circ$ and* `IFLAG_H(12)`= 5. *We note that $|D^{H^0}_{44}(\hat{s})| = 1$. The three Higgs-boson pole masses are indicated by thin vertical lines.*

In situations where two or more MSSM Higgs bosons contribute simultaneously to a process, the transitions between the Higgs-boson mass eigenstates need to be considered before their decays. For this reason, we include the *complete* 4×4-dimensional propagator matrix $D^{H^0}(\hat{s})$ spanned by the basis (H_1, H_2, H_3, G^0) [10], including off-diagonal absorptive parts [9]. The dimensionless neutral Higgs-boson propagator matrix is given by

$$D^{H^0}(\hat{s}) \; = \; \hat{s} \begin{pmatrix} \hat{s}-M_{H_1}^2+i\Im\mathrm{m}\widehat{\Pi}_{11}(\hat{s}) & i\Im\mathrm{m}\widehat{\Pi}_{12}(\hat{s}) & i\Im\mathrm{m}\widehat{\Pi}_{13}(\hat{s}) & i\Im\mathrm{m}\widehat{\Pi}_{14}(\hat{s}) \\ i\Im\mathrm{m}\widehat{\Pi}_{21}(\hat{s}) & \hat{s}-M_{H_2}^2+i\Im\mathrm{m}\widehat{\Pi}_{22}(\hat{s}) & i\Im\mathrm{m}\widehat{\Pi}_{23}(\hat{s}) & i\Im\mathrm{m}\widehat{\Pi}_{24}(\hat{s}) \\ i\Im\mathrm{m}\widehat{\Pi}_{31}(\hat{s}) & i\Im\mathrm{m}\widehat{\Pi}_{32}(\hat{s}) & \hat{s}-M_{H_3}^2+i\Im\mathrm{m}\widehat{\Pi}_{33}(\hat{s}) & i\Im\mathrm{m}\widehat{\Pi}_{34}(\hat{s}) \\ i\Im\mathrm{m}\widehat{\Pi}_{41}(\hat{s}) & i\Im\mathrm{m}\widehat{\Pi}_{42}(\hat{s}) & i\Im\mathrm{m}\widehat{\Pi}_{43}(\hat{s}) & \hat{s}+i\Im\mathrm{m}\widehat{\Pi}_{44}(\hat{s}) \end{pmatrix}^{-1}, \tag{1}$$

where $M_{H_{1,2,3}}$ are the one-loop Higgs-boson pole masses, and higher-order absorptive effects on $M_{H_{1,2,3}}$ have been ignored [6]. The label '4' refers to the would-be Goldstone boson of the Z boson. The absorptive part of the Higgs-boson propagator matrix receives contributions from loops of fermions, vector bosons, associated pairs of Higgs and vector bosons, Higgs-boson pairs, and sfermions:

$$\Im\mathrm{m}\widehat{\Pi}_{ij}(\hat{s}) = \Im\mathrm{m}\widehat{\Pi}_{ij}^{ff}(\hat{s}) + \Im\mathrm{m}\widehat{\Pi}_{ij}^{VV}(\hat{s}) + \Im\mathrm{m}\widehat{\Pi}_{ij}^{HV}(\hat{s}) + \Im\mathrm{m}\widehat{\Pi}_{ij}^{HH}(\hat{s}) + \Im\mathrm{m}\widehat{\Pi}_{ij}^{\tilde{f}\tilde{f}}(\hat{s})\,, \tag{2}$$

respectively. We refer to Ref. [9] for their explicit expressions. For the Goldstone-Higgs mixings, $\Im\mathrm{m}\widehat{\Pi}_{i4,4i}$ and $\Im\mathrm{m}\widehat{\Pi}_{44}$, we take the leading contributions ignoring all gauge-coupling mediated parts. We also include the 2×2-dimensional propagator matrix for the charged Higgs bosons $D^{H^\pm}(\hat{s})$ spanned by the basis $(H^\pm, G^\pm)$, including off-diagonal absorptive parts:

$$D^{H^\pm}(\hat{s}) = \hat{s} \begin{pmatrix} \hat{s}-M_{H^\pm}^2+i\Im\mathrm{m}\widehat{\Pi}_{H^\pm H^\pm}(\hat{s}) & i\Im\mathrm{m}\widehat{\Pi}_{H^\pm G^\pm}(\hat{s}) \\ i\Im\mathrm{m}\widehat{\Pi}_{G^\pm H^\pm}(\hat{s}) & \hat{s}+i\Im\mathrm{m}\widehat{\Pi}_{G^\pm G^\pm}(\hat{s}) \end{pmatrix}^{-1}. \tag{3}$$

The relevant Goldstone-boson couplings are given in Appendix B. For the 16 elements of the neutral Higgs-boson propagator matrix $D^{H^0}(\hat{s})$ and for the 4 elements of the charged Higgs-boson propagator matrix $D^{H^\pm}(\hat{s})$, the slots `CAUX_H(100-119)` are used as shown in Table 2. In Fig. 3, as an example, we show the absolute value of all components of the Higgs-boson propagator matrix $D^{H^0}(\hat{s})$ as functions of $\sqrt{\hat{s}}$ for the trimixing scenario with $\Phi_A = -\Phi_3 = 90^\circ$.

It is important to remark that the 4×4 propagator matrix (1) is sufficient to encode all $H_i{-}Z$- and $G^0{-}Z$ mixing effects within the Pinch Technique (PT) framework [10,11], which has been adopted here to remove consistently gauge-dependent and high-energy unitarity-violating terms from $\Im\mathrm{m}\widehat{\Pi}_{ij}(\hat{s})$ [9]. For example, the self-energy transition $H_i \to Z_\mu$, $\widehat{\Pi}^\mu_{ZH_i} = p^\mu \widehat{\Pi}_{ZH_i}$, is related to $\widehat{\Pi}_{G^0H_i}$ through

$$\hat{s}\,\widehat{\Pi}_{ZH_i}(\hat{s}) \;=\; -\,i\,M_Z^2\,\widehat{\Pi}_{G^0H_i}(\hat{s})\,, \tag{4}$$

with $\hat{s} = p^2$. We recall that the self-energy transitions $H_i \to \gamma$ and $G^0 \to \gamma$ are completely absent within the PT framework. More details may be found in [10].

Note that the elements of the propagator matrix depend on the center-of-mass energy, denoted by $\sqrt{\hat{s}}$, which is stored in `RAUX_H(101)`, see Table 1. Along with $D^{H^0,H^\pm}(\hat{s})$, the

$\hat{s}$-dependent couplings of the neutral Higgs bosons to two gluons, $S_i^g(\sqrt{\hat{s}})$ and $P_i^g(\sqrt{\hat{s}})$, and two photons, $S_i^\gamma(\sqrt{\hat{s}})$ and $P_i^\gamma(\sqrt{\hat{s}})$, are needed when we consider the production of the neutral Higgs bosons at the LHC [9] and a $\gamma\gamma$ collider [12]. They are calculated and stored in `CAUX_H(130-135)` and `CAUX_H(140-145)` as shown in Table 2. Two additional flags are used to control the inclusion of the off-diagonal absorptive parts and print out the the $\hat{s}$-dependent propagator matrix and the $\hat{s}$-dependent Higgs couplings to two photons and gluons:

- `IFLAG_H(13)`$=1$: Does not include the off-diagonal absorptive parts in the propagator matrices $D^{H^0,H^\pm}(\hat{s})$.
- `IFLAG_H(14)`$=1$: Prints out each component of the Higgs-boson propagator matrices $D^{H^0,H^\pm}(\hat{s})$ and the $\hat{s}$-dependent couplings $S_i^{\gamma,g}(\sqrt{\hat{s}})$ and $P_i^{\gamma,g}(\sqrt{\hat{s}})$.

2.2 Improved Treatment of Higgs-Boson Couplings and Decays

The main updates include:

- The electroweak corrections to the neutral Higgs couplings to pairs of tau leptons and b-quarks [13]. The corrections to the Yukawa couplings and the couplings of H_i to the scalar and pseudoscalar fermion bilinears are calculated as in Eqs.(A.1)-(A.2) of Ref. [3]. For details, we refer to Ref. [9].
- The three-body decay $H^+ \to t^*\bar{b} \to W^+ b\bar{b}$. The decay width is given by

$$\Gamma(H^+ \to W^+ b\bar{b}) = N_C \frac{g^2\, g_{tb}^2\, M_{H^\pm}}{512\pi^3} \int_0^{1-\kappa_W} \mathrm{d}x_1 \int_{1-\kappa_W-x_1}^{1-\frac{\kappa_W}{1-x_1}} \mathrm{d}x_2 \frac{F(x_1,x_2)}{(1-x_2-\kappa_t+\kappa_b)^2+\kappa_t\gamma_t}, \quad (5)$$

where $\kappa_x \equiv m_x^2/M_{H^\pm}^2$, $\gamma_t \equiv \Gamma_t^2/M_{H^\pm}^2$ and $x_i \equiv 2E_i/M_{H^\pm}$ with E_1 and E_2 being the energies of the b and $\bar{b}$ quarks, respectively. In the charged Higgs-boson rest frame, the function $F(x_1,x_2)$ is given by

$$\begin{aligned} F(x_1,x_2) = & \Bigg\{ |g_L|^2 \Bigg[\kappa_t \bigg(\frac{(1-x_1)(1-x_2)}{\kappa_W} + 2x_1 + 2x_2 - 3 + 2\kappa_W \bigg) - 2\kappa_b\kappa_t \Bigg] \\ & + |g_R|^2 \Bigg[\frac{x_2^3 + x_1x_2^2 - 3x_2^2 - 2x_1x_2 + 3x_2 + x_1 - 1}{\kappa_W} \\ & \quad + (x_2^2 + 2x_1x_2 - 4x_2 - 2x_1 + 3 - 2\kappa_W) \\ & \quad + \kappa_b \bigg(-2x_1 + 3 + 2\kappa_W + \frac{-2x_2^2 - x_1x_2 + 5x_2 + x_1 - 3}{\kappa_W} \bigg) - 2\kappa_b^2 \Bigg] \\ & + 2\sqrt{\kappa_b\kappa_t}\, \Re\mathrm{e}(g_L g_R^*) \Bigg[\frac{(x_2-1)^2}{\kappa_W} + (-x_2 + 1 - 2\kappa_W) + 2\kappa_b \Bigg] \Bigg\}, \end{aligned} \quad (6)$$

where $g_L \equiv g^S_{H^+\bar{t}b} - i g^P_{H^+\bar{t}b}$ and $g_R \equiv g^S_{H^+\bar{t}b} + i g^P_{H^+\bar{t}b}$.

- The contributions from tau-lepton and charm-quark loops to the couplings $S_i^\gamma(M_{H_i})$ and $P_i^\gamma(M_{H_i})$.
- A new flag `IFLAG_H(57)`$=1$: This is an error message that appears when one of the magnitudes of the complex input parameters is negative.

The `CPsuperH` homepage has been continuously brought up to date after its first appearance to include the updates discussed in this subsection and others not mentioned here. We refer to the file `OLIST_V1` for a full list of updates to the original version which can be found in the `CPsuperH` homepage.

3 Higgs-Mediated Two-Loop Electric Dipole Moments

The CP phases in the MSSM are significantly constrained by measurements of Electric Dipole Moments (EDMs). In particular, the EDM of the Thallium atom may provide currently the most stringent constraint on MSSM scenarios with explicit CP violation. The atomic EDM of ^{205}Tl gets its main contributions from two terms [14, 15]:

$$\begin{aligned} d_{\rm Tl}\,[e\,cm] &= -585\cdot d_e\,[e\,cm] \;-\; 8.5\times 10^{-19}\,[e\,cm]\cdot(C_S\,{\rm TeV}^2)+\cdots\,, \\ &\equiv (d_{\rm Tl})^e\,[e\,cm]+(d_{\rm Tl})^{C_S}\,[e\,cm]+\cdots\,, \end{aligned} \tag{7}$$

where d_e denotes the electron EDM and C_S is the coefficient of the CP-odd electron-nucleon interaction $\mathcal{L}_{C_S} = C_S\,\bar{e}i\gamma_5 e\,\bar{N}N$. The dots denote sub-dominant contributions from 6-dimensional tensor and higher-dimensional operators.

The contributions of the first- and second-generation phases, $\Phi_{A_{e,\mu}}$ and $\Phi_{A_{d,s}}$, to EDMs can be drastically reduced either by assuming that these phases sufficiently small, or if the first- and second-generation squarks and sleptons are sufficiently heavy. However, even when the contributions of the first and second generation phases to EDMs are suppressed, there are still sizeable contributions to EDMs from Higgs-mediated two-loop diagrams [16].

The Higgs-mediated two-loop Thallium ($d^H_{\rm Tl}$), electron (d^H_e), and muon (d^H_μ) EDMs are calculated and stored in `RAUX_H(111-120)` as shown in Table 1. The Thallium and electron EDMs consist of:

$$\begin{aligned} d^H_{\rm Tl} &= (d^H_{\rm Tl})^e + (d^H_{\rm Tl})^{C_S}\,, \\ d^H_e &= (d^H_e)^{\tilde{t}} + (d^H_e)^{\tilde{b}} + (d^H_e)^{t} + (d^H_e)^{b} + (d^H_e)^{\tilde{\chi}^\pm}\,. \end{aligned} \tag{8}$$

The explicit expressions for the EDMs in the `CPsuperH` conventions and notations may be found in Ref. [17]. A flag `IFLAG_H(15)`$=1$ is used to print out the results of the EDM calculations:

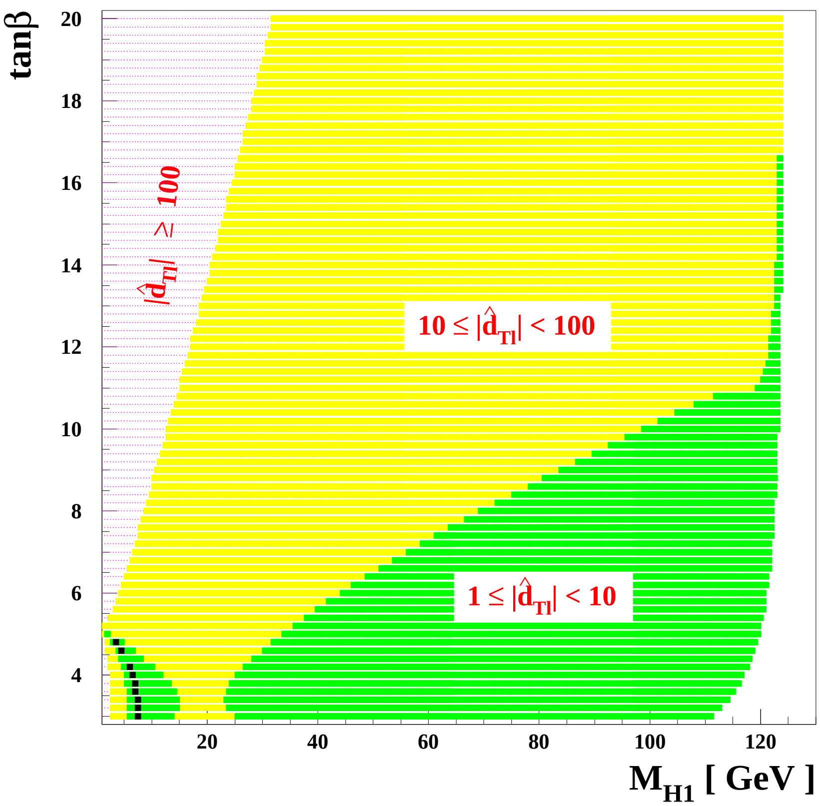

Figure 4: *The Thallium EDM* $\hat{d}_{\rm Tl} \equiv d^H_{\rm Tl} \times 10^{24}$ $[e\,cm]$ *in the CPX scenario with* $\Phi_A = \Phi_3 = 90^\circ$ *and* $M_{\rm SUSY} = 0.5$ *TeV taking* `IFLAG_H(12)`$= 5$ *[18]. The different shaded regions correspond to different ranges of* $|\hat{d}_{\rm Tl}|$ *as shown. Specially, in the narrow region denoted by black squares, one has* $|\hat{d}_{\rm Tl}| < 1$*, consistent with the current Thallium EDM constraint.*

- `IFLAG_H(15)`$= 1$: Print out EDMs.

In Fig. 4, we show the rescaled Thallium EDM $\hat{d}_{\rm Tl} \equiv d^H_{\rm Tl} \times 10^{24}$ in units of $e\,cm$ in the $\tan\beta$-M_{H_1} plane, in the CPX scenario with `IFLAG_H(12)`$= 5$. We observe, when $\tan\beta \lesssim 5$ and $M_{H_1} \lesssim 10$ GeV, one may have $|\hat{d}_{\rm Tl}| < 1$ in the narrow region denoted by black squares which is consistent with the current 2-σ upper bound on the Thallium EDM [19]: $|d_{\rm Tl}| \lesssim 1.3 \times 10^{-24}\,[e\,cm]$. We note that the region 8 GeV $\lesssim M_{H_1} \lesssim 10$ GeV with $\tan\beta \lesssim 10$ has not been excluded by the combined constraints from the LEP searches [20] and the $\Upsilon(1S) \to \gamma H_1$ decay [21].

In the future, this treatment of the most important two-loop contributions to the Thallium EDM will be supplemented by a more complete implementation of calculations of the well-known one-oop contributions to this and other EDMs.

4 B-Meson Observables

An important innovation in `CPsuperH2.0` is the inclusion of the following important Higgs-mediated B-meson observables:

- The branching ratio of B_s meson into a pair of muons: $B(B_s \to \mu\mu)$,
- The branching ratio of B_d meson into a pair of tau leptons: $B(B_d \to \tau\tau)$,
- The SUSY contribution to the B_d^0-$\bar{B}_d^0$ mass difference: $\Delta M_{B_d}^{\rm SUSY}$,
- The SUSY contribution to the B_s^0-$\bar{B}_s^0$ mass difference: $\Delta M_{B_s}^{\rm SUSY}$,
- The ratio of the branching ratio $B(B_u \to \tau\nu)$ to the SM value:

$$R_{B\tau\nu} = \frac{B(B_u^- \to \tau\nu)}{B^{\rm SM}(B_u^- \to \tau\nu)}$$

,

- The branching ratio $B(B \to X_s\gamma)$ and the direct CP asymmetry $\mathcal{A}_{\rm CP}(B \to X_s\gamma)$.

We adopt the most recent gauge-invariant and flavour-covariant formalism to calculate the flavour-changing effective Lagrangian for the interactions of the neutral and charged Higgs fields to the up- and down-type quarks including a new class of dominant subleading contributions [5]. In the current version, the single-Higgs insertion approximation is used.

For the calculations of B-meson observables, the array `SMPARA_H` for the SM parameters has been extended to include information on the CKM matrix, parameterized via λ, A, $\bar\rho$, and $\bar\eta$, as seen in Table 3. The CKM matrix is constructed as [22]

$$V = \left(\begin{array}{ccc} c_{12}\, c_{13} & s_{12}\, c_{13} & s_{13}\, e^{-i\,\delta} \\ -s_{12}\, c_{23} - c_{12}\, s_{23}\, s_{13}\, e^{i\,\delta} & c_{12}\, c_{23} - s_{12}\, s_{23}\, s_{13}\, e^{i\,\delta} & s_{23}\, c_{13} \\ s_{12}\, s_{23} - c_{12}\, c_{23}\, s_{13}\, e^{i\,\delta} & -c_{12}\, s_{23} - s_{12}\, c_{23}\, s_{13}\, e^{i\,\delta} & c_{23}\, c_{13} \end{array} \right) , \tag{9}$$

where $s_{ij} = \sin\theta_{ij}$, $c_{ij} = \cos\theta_{ij}$, and δ is the KM phase with $s_{ij}\,, c_{ij} \geq 0$. In terms of λ, A, $\bar\rho$, and $\bar\eta$, they are given by

$$s_{12} = \lambda\,, \quad s_{23} = A\lambda^2\,, \quad s_{13}\, e^{i\,\delta} = \frac{A\lambda^3(\bar\rho + i\,\bar\eta)\sqrt{1-A^2\lambda^4}}{\sqrt{1-\lambda^2}\,[1 - A^2\lambda^4(\bar\rho + i\,\bar\eta)]}\,, \tag{10}$$

and $c_{ij} = \sqrt{1-|s_{ij}|^2}$. The SUSY parameter array `SSPARA_H` is also extended to include the hierarchy factors $\rho_{\tilde{Q},\tilde{U},\tilde{D},\tilde{L},\tilde{E}}$ between the first two and third generations [23], see Table 4.

In the super-CKM basis, the 3×3 squark mass matrices squared are taken to be diagonal:

$$
\begin{aligned}
\widetilde{\mathbf{M}}_Q^2 &= m_{\tilde{Q}_3}^2 \times \operatorname{diag}(\rho_{\tilde{Q}}^2, \rho_{\tilde{Q}}^2, 1)\,, \\
\widetilde{\mathbf{M}}_U^2 &= m_{\tilde{U}_3}^2 \times \operatorname{diag}(\rho_{\tilde{U}}^2, \rho_{\tilde{U}}^2, 1)\,, \\
\widetilde{\mathbf{M}}_D^2 &= m_{\tilde{D}_3}^2 \times \operatorname{diag}(\rho_{\tilde{D}}^2, \rho_{\tilde{D}}^2, 1)\,, \\
\widetilde{\mathbf{M}}_L^2 &= m_{\tilde{L}_3}^2 \times \operatorname{diag}(\rho_{\tilde{L}}^2, \rho_{\tilde{L}}^2, 1)\,, \\
\widetilde{\mathbf{M}}_E^2 &= m_{\tilde{E}_3}^2 \times \operatorname{diag}(\rho_{\tilde{E}}^2, \rho_{\tilde{E}}^2, 1)\,.
\end{aligned}
\tag{11}
$$

Finally, the results for the B-meson observables are stored in `RAUX_H(130-136)` as shown in Table 1. The SUSY contributions to the $\Delta B = 2$ transition amplitudes are stored in `CAUX_H(150)` and `CAUX_H(151)`, see Table 1. Note the relations `RAUX_H(132)` $=$ $2 \times |$`CAUX_H(150)`$|$ and `RAUX_H(133)` $= 2 \times |$`CAUX_H(151)`$|$. Two flags `IFLAG_H(16)` and `IFLAG_H(17)` are used to print out the results of the calculation of B-meson observables:

- `IFLAG_H(16)`$= 1$: Print out B-meson observables.
- `IFLAG_H(17)`$= 1$: Print out details of the $B \to X_s\gamma$ calculation.

For numerical examples of B-meson observables, we take the CPX scenario [8] with $M_{\rm SUSY} = 0.5$ TeV and the common A-term phase $\Phi_A \equiv \Phi_{A_t} = \Phi_{A_t} = \Phi_{A_\tau}$ in the convention $\Phi_\mu = 0^\circ$. We take account of the dependence on the hierarchy factors $\rho_{\tilde{Q},\tilde{U},\tilde{D}}$ between the first two and the third generations, taking a common value ρ for the three of them.

Figure 5 shows the dependence of the branching ratio $B(B_s \to \mu^+\mu^-)$ on the phase of the gluino mass parameter Φ_3 for four values of $\tan\beta$. The charged Higgs-boson pole mass is fixed at $M_{H^\pm} = 200$ GeV. In each frame, two sets of three lines are shown. The upper lines are for higher $\rho = 10$ and the lower ones for $\rho = 1$. For fixed ρ, three lines show the cases of $\Phi_A = 0^\circ$ (solid), 90° (dashed), and 180° (dash-dotted). The ρ dependence is shown in Fig. 6. We clearly see the *GIM operative point* mechanism discussed in Ref. [23] around $\rho \sim 1.2$ when $(\Phi_3\,, \Phi_A) = (0^\circ\,, 180^\circ)$ (solid lines). Figure 7 shows the rescaled branching ratio $\widehat{B}_\mu \equiv B(B_s \to \mu^+\mu^-) \times 10^7$ in the M_{H_1}-$\tan\beta$ plane when the phases are fixed at $\Phi_A = \Phi_3 = 90^\circ$. The unshaded region is not theoretically allowed. Only the region with $\widehat{B}_\mu < 0.58$ is consistent with the current experimental upper limit at 95 % C.L., corresponding to $\tan\beta \lesssim 20\,(8)$ for $\rho = 1\,(10)$.

The rescaled branching ratio $\widehat{B}_{s\gamma} \equiv B(B \to X_s\gamma) \times 10^4$ is shown in Fig. 8. In contrast to the $B_s \to \mu^+\mu^-$ case, we observe that higher $\tan\beta$ region is experimentally allowed: $\tan\beta \gtrsim 35\,(20)$ for $\rho = 1\,(10)$. This is because the charged-Higgs contribution is suppressed due to the threshold corrections when $\tan\beta$ is large. The charged-Higgs contribution to $B \to X_s\gamma$ is proportional to $1/(1 + |\kappa|^2 \tan^2\beta)$ [26], where κ represents the threshold corrections with $|\kappa| \simeq 0.05$ for the parameters chosen [27].

Figure 9 shows the ratio of the branching ratio $B(B_u \to \tau\nu)$ to its SM value, $R_{B\tau\nu}$. In the left frame with $\rho = 1$, we see two connected bands of the experimentally allowed 1-σ region, $0.62 < R_{B\tau\nu} < 1.38$. If we consider the 2-$\sigma$ limit, only the upper-left region with $M_{H_1} \lesssim 95$ GeV and $\tan\beta \gtrsim 35$ is not allowed. For larger $\rho = 10$, the allowed region becomes narrower.

In Fig. 10, we show the region satisfying the experimental constraints from $B(B_s \to \mu^+\mu^-)$ (95 %), $B(B \to X_s\gamma)$ (2 σ), and $R_{B\tau\nu}$ (1 σ). First we observe that there is no region that satisfies the $B_s \to \mu^+\mu^-$ and $B \to X_s\gamma$ constraints simultaneously for both $\rho = 1$ and 10. If one neglects the constraint from $B(B_s \to \mu^+\mu^-)$, only the high-$\tan\beta$ region would remain. Taking account of $B_u \to \tau\nu$ constraint, the region with $\tan\beta \gtrsim 36$ and $M_{H_1} \gtrsim 80$ GeV is allowed when $\rho = 1$. On the other hand, neglecting the constraint from $B(B \to X_s\gamma)$, the allowed region is constrained in the parameter space with $\tan\beta \lesssim 20$ and $M_{H_1} \gtrsim 10$ GeV for $\rho = 1$. For $\rho = 10$, the $B \to X_s\gamma$ constraint is relaxed but those from $B(B_s \to \mu^+\mu^-)$ and $R_{B\tau\nu}$ become more stringent.

Finally, in Fig. 11, we show the region allowed experimentally by the measurement $B(B_d \to \tau^+\tau^-) < 4.1 \times 10^{-3}$ (90 %) [29] (upper frames) and the regions where the SUSY contribution is smaller than the measured values of B_s^0-$\bar{B}_s^0$ mass difference [30] (middle frames) and B_d^0-$\bar{B}_d^0$ mass difference [22] (lower frames). We see that the $B(B_d \to \tau^+\tau^-)$ constraint has the least impact on these parameter planes, whereas the impacts of the B_s^0-$\bar{B}_s^0$ and B_d^0-$\bar{B}_d^0$ mass differences are similar.

These examples illustrate the possible interplays between the different B-meson observables, and how they may vary significantly with the values of the CP-violating phases. `CPsuperH2.0` provides a unique tool for combining these constraints and pursuing their implications for other oberservables. In the future, the `CPsuperH2.0` treatment of these important B-meson observables will be supplemented by the implementation of calculations of other flavour observables, including the K sector.

5 Summary and Outlook

We have presented in this paper a description of the new features of the Fortran code `CPsuperH2.0`. In addition to improved calculations of the Higgs-boson poles masses with more complete treatment of threshold effects in self-energies and Yukawa couplings, the *complete* 4×4 (2×2) neutral (charged) Higgs-boson propagator matrices with the Goldstone-Higgs mixing effects have been consistently implemented. Specifically, the neutral Higgs-boson propagator matrix constitutes a necessary ingredient for the studies of a system of strongly-mixed Higgs bosons at colliders together with the center-of-mass dependent Higgs-boson couplings to gluons and photons. It also provides the improved Higgs-boson couplings to tau leptons, b quarks, and two photons. The important three-body decay

$H^+ \to t^*\bar{b} \to W^+ b\bar{b}$ is included.

In order to provide a more complete, consistent tool for calculating CP-violating observables in the MSSM, and specifically to incorporate the important constraints coming from precision experiments at low energies, `CPsuperH2.0` has been extended to include a number of B-meson observables, as well as the Higgs-mediated two-loop contributions to EDMs of the Thallium atom, electron and muon. The currently available B-meson observables are the branching ratios of $B_s \to \mu^+\mu^-$, $B_d \to \tau^+\tau^-$, $B_u \to \tau\nu$, $B \to X_s\gamma$ and the latter's CP-violating asymmetry $\mathcal{A}_{\rm CP}$, and the supersymmetric contributions to the $B^0_{s,d} - \bar{B}^0_{s,d}$ mass differences. Further low-energy observables are to be included in future updates.

The improved Fortran code `CPsuperH2.0` provides a coherent and complete numerical framework in which one can calculate consistently observables in both low- and high-energy experiments probing physics beyond the SM.

Acknowledgements

The work of J.S.L. was supported in part by the Korea Research Foundation and the Korean Federation of Science and Technology Societies Grant funded by the Korea Government (MOEHRD, Basic Research Promotion Fund) and in part by the National Science Coundcil of Taiwan, R.O.C. under Grant No. NSC 96-2811-M-008-068. The work of A.P. was support in part by the STFC research grant: PP/D000157/1. Work at ANL is supported in part by the US DOE, Div. of HEP, Contract DE-AC02-06CH11357 . Fermilab is operated by Universities Research Association Inc. under contract no. DE-AC02-76CH02000 with the DOE. We thank S.Y. Choi and M. Drees for past collaboration on `CPsuperH`, and for discussions on this updated version.

A List of changes

Here we summarize the improved features introduced in `CPsuperH2.0` compared to the prior version of `CPsuperH`.

- New common blocks:
  - `COMMON /HC_RAUX/ RAUX_H(NAUX=999)`, see Table 1
  - `COMMON /HC_CAUX/ CAUX_H(NAUX=999)`, see Table 2
- Extended arrays for input parameters:
  - `SMPARA_H(NSMIN=19)`, see Table 3
  - `SMPARA_H(NSSIN=26)`, see Table 4
- New names for improved `FORTRAN` files:
  - `cpsuperh.f` $\longrightarrow$ `cpsuperh2.f`
  - `fillpara.f` $\longrightarrow$ `fillpara2.f`
  - `fillhiggs.f` $\longrightarrow$ `fillhiggs2.f`
  - `fillcoupl.f` $\longrightarrow$ `fillcoupl2.f`
  - `fillgambr.f` $\longrightarrow$ `fillgambr2.f`
- New `FORTRAN` files:
  - `filldhpg.f` is to calculate the full propagator matrices $D^{H^0,H^\pm}(\hat{s})$ and the $\hat{s}$-dependent couplings $S_i^{g,\gamma}(\sqrt{\hat{s}})$ and $P_i^{g,\gamma}(\sqrt{\hat{s}})$.
  - `higgsedm.f` is to calculate Higgs-mediated two-loop EDMs of Thallium, electron, and muon.
  - `fillbobs.f` is to calculate the B-meson observables: $B(B_s \to \mu\mu)$, $B(B_d \to \tau\tau)$, $\Delta M_{B_d}^{\rm SUSY}$, $\Delta M_{B_s}^{\rm SUSY}$, $R_{B\tau\nu}$, $B(B \to X_s\gamma)$, and $\mathcal{A}_{\rm CP}(B \to X_s\gamma)$.
- New flags:
  - `IFLAG_H(12)` $=$ `0` $-$ `5`: For the level of improvement in the calculation of the Higgs-boson pole masses.
  - `IFLAG_H(13)` $=$ `1`: Not to include the off-diagonal absorptive parts in the propagator matrices $D^{H^0,H^\pm}(\hat{s})$.
  - `IFLAG_H(14)` $=$ `1`: Print out the the elements of the full propagator matrices $D^{H^0,H^\pm}(\hat{s})$ and the $\hat{s}$-dependent couplings $S_i^{g,\gamma}(\sqrt{\hat{s}})$ and $P_i^{g,\gamma}(\sqrt{\hat{s}})$.

– `IFLAG_H(15) = 1`: Print out EDMs.

– `IFLAG_H(16) = 1`: Print out B-meson observables.

– `IFLAG_H(17) = 1`: Print out $B \to X_s \gamma$ details.

– `IFLAG_H(57) = 1`: This is an error message that appears when one of the magnitudes of the complex SUSY input parameters is negative.

– `IFLAG_H(60) = 1`: This is an error message that appears when the iterative method for the neutral Higgs-boson pole masses fails.

B Goldstone-boson couplings to third-generation fermions and sfermions

Here we present the Goldstone-(s)fermion-(s)fermion couplings in the `CPsuperH` convention.

- $\underline{G^0\text{-}\bar{f}\text{-}f}$

$$\mathcal{L}_{G^0\bar{f}f} = -\sum_{f=t,b,\tau} \frac{g\, m_f}{2M_W}\, G^0\, \bar{f}\left(i\, g^P_{G^0\bar{f}f}\, \gamma_5\right) f\,, \tag{B.1}$$

where

$$g^P_{G^0\bar{t}t} = -1\,, \quad g^P_{G^0\bar{b}b} = g^P_{G^0\bar{\tau}\tau} = +1\,. \tag{B.2}$$

- $\underline{G^\pm\text{-}\bar{f}\text{-}f'}$

$$\begin{aligned} \mathcal{L}_{G^\pm\bar{f}f'} &= \frac{g}{\sqrt{2}M_W} \sum_{(f_\uparrow,f_\downarrow)=(t,b),(\nu,\tau)} G^+\, \bar{f}_\uparrow \left(m_{f_\uparrow}\, P_L \;-\; m_{f_\downarrow}\, P_R \right) f_\downarrow \;+\; \text{h.c.} \\ &= -g_{tb}\, G^+\, \bar{t}\,(g^S_{G^+\bar{t}b} + i g^P_{G^+\bar{t}b}\gamma_5)\, b - g_{\nu_\tau\tau}\, G^+\, \bar{\nu}_\tau\, (g^S_{G^+\bar{\nu}_\tau\tau} + i g^P_{G^+\bar{\nu}_\tau\tau}\gamma_5)\, \tau \;+\; \text{h.c.}\,, \end{aligned} \tag{B.3}$$

where

$$\begin{aligned} g_{tb} &= -\frac{g\, m_t}{\sqrt{2}M_W}\,, \quad g^S_{G^+\bar{t}b} = \frac{1 - m_b/m_t}{2}\,, \quad g^P_{G^+\bar{t}b} = i\,\frac{1 + m_b/m_t}{2}\,; \\ g_{\nu_\tau\tau} &= -\frac{g\, m_\tau}{\sqrt{2}M_W}\,, \quad g^S_{G^+\bar{\nu}_\tau\tau} = -\frac{1}{2}\,, \qquad g^P_{G^+\bar{\nu}_\tau\tau} = i\,\frac{1}{2}\,. \end{aligned} \tag{B.4}$$

- $\underline{G^0\text{-}\tilde{f}^*\text{-}\tilde{f}}$

$$\mathcal{L}_{G^0\tilde{f}\tilde{f}} = v \sum_{f=t,b,\tau} g_{G^0\tilde{f}^*_i\tilde{f}_j}\, (G^0\, \tilde{f}^*_i\, \tilde{f}_j)\,, \tag{B.5}$$

where

$$v\, g_{G^0\tilde{f}^*_i\tilde{f}_j} = \left(\Gamma^{G^0\tilde{f}^*\tilde{f}}\right)_{\alpha\beta} U^{\tilde{f}*}_{\alpha i} U^{\tilde{f}}_{\beta j}\,. \tag{B.6}$$

The couplings in the weak-interaction basis are given by

$$
\begin{aligned}
\Gamma^{G^0\tilde{t}^*\tilde{t}} &= \frac{1}{\sqrt{2}}\left(\begin{array}{cc} 0 & i\,h_t^*(s_\beta A_t^* - c_\beta\mu) \\ -i\,h_t(s_\beta A_t - c_\beta\mu^*) & 0 \end{array}\right), \\
\Gamma^{G^0\tilde{b}^*\tilde{b}} &= \frac{1}{\sqrt{2}}\left(\begin{array}{cc} 0 & -i\,h_b^*(c_\beta A_b^* - s_\beta\mu) \\ i\,h_b(c_\beta A_b - s_\beta\mu^*) & 0 \end{array}\right), \\
\Gamma^{G^0\tilde{\tau}^*\tilde{\tau}} &= \frac{1}{\sqrt{2}}\left(\begin{array}{cc} 0 & -i\,h_\tau^*(c_\beta A_\tau^* - s_\beta\mu) \\ i\,h_\tau(c_\beta A_\tau - s_\beta\mu^*) & 0 \end{array}\right). \qquad \text{(B.7)}
\end{aligned}
$$

- $\underline{G^\pm\text{-}\tilde{f}^*\text{-}\tilde{f}'}$

$$
\mathcal{L}_{G^\pm\tilde{f}\tilde{f}'} = v\,g_{G^+\tilde{t}_i^*\tilde{b}_j}(G^+\,\tilde{t}_i^*\,\tilde{b}_j) \,+\, v\,g_{G^+\tilde{\nu}_\tau^*\tilde{\tau}_i}(G^+\,\tilde{\nu}_\tau^*\,\tilde{\tau}_i) \,+\text{h.c.}\,, \qquad \text{(B.8)}
$$

where

$$
v\,g_{G^+\tilde{t}_i^*\tilde{b}_j} = \left(\Gamma^{G^+\tilde{t}^*\tilde{b}}\right)_{\alpha\beta} U^{\tilde{t}*}_{\alpha i} U^{\tilde{b}}_{\beta j} \quad \text{and} \quad v\,g_{G^+\tilde{\nu}_\tau^*\tilde{\tau}_i} = \Gamma^{G^+\tilde{\nu}_\tau^*\tilde{\tau}_\alpha}\,U^{\tilde{\tau}}_{\alpha i}\,. \qquad \text{(B.9)}
$$

The couplings in the weak-interaction basis are given by

$$
\begin{aligned}
\Gamma^{G^+\tilde{t}^*\tilde{b}} &= \left(\begin{array}{cc} \frac{1}{\sqrt{2}}\left(|h_u|^2 s_\beta^2 - |h_d|^2 c_\beta^2\right) v \,+\, \frac{1}{2\sqrt{2}}\,g^2 c_{2\beta}\,v & -h_d^*\,(c_\beta A_d^* - s_\beta\mu) \\ h_u\,(s_\beta A_u - c_\beta\mu^*) & 0 \end{array}\right), \\
\Gamma^{G^+\tilde{\nu}_\tau^*\tilde{\tau}_L} &= -\frac{1}{\sqrt{2}}\,|h_\tau|^2 c_\beta^2\,v \,+\, \frac{1}{2\sqrt{2}}\,g^2 c_{2\beta}\,v\,, \\
\Gamma^{G^+\tilde{\nu}_\tau^*\tilde{\tau}_R} &= -h_\tau^*\,(c_\beta A_\tau^* - s_\beta\mu)\,. \qquad \text{(B.10)}
\end{aligned}
$$

C Sample new outputs

Here we show the new outputs of `CPsuperH2.0` for the CPX scenario with $\tan\beta = 5$, $M_{H^\pm} = 300$ GeV, $M_{\rm SUSY} = 500$ GeV, and $\Phi_A = \Phi_3 = 90°$.

- `IFLAG_H(1) = 1`: In the new version, we are using $m_b(m_t^{\rm pole}) = 3.155$ GeV and $m_c(m_t^{\rm pole}) = 0.735$ GeV as defaults. Note also that the list of the SM and SUSY input parameters is extended to include the CKM matrix and the diagonal sfermion mass matrices.

```
---------------------------------------------------------
 Standard Model Parameters  in /HC_SMPARA/
---------------------------------------------------------
 AEM_H    = 0.7812E-02 : alpha_em(MZ)
 ASMZ_H   = 0.1185E+00 : alpha_s(MZ)
 MZ_H     = 0.9119E+02 : Z boson mass in GeV
 SW_H     = 0.4808E+00 : sinTheta_W
 ME_H     = 0.5000E-03 : electron mass in GeV
```

```
MMU_H    = 0.1065E+00 : muon mass in GeV
MTAU_H   = 0.1777E+01 : tau mass in GeV
MDMT_H   = 0.4000E-02 : d-quark mass at M_t^pole in GeV
MSMT_H   = 0.9000E-01 : s-quark mass at M_t^pole in GeV
MBMT_H   = 0.3155E+01 : b-quark mass at M_t^pole in GeV
MUMT_H   = 0.2000E-02 : u-quark mass at M_t^pole in GeV
MCMT_H   = 0.7350E+00 : c-quark mass at M_t^pole in GeV
MTPOLE_H = 0.1743E+03 : t-quark pole mass in GeV
GAMW_H   = 0.2118E+01 : Gam_W in GeV
GAMZ_H   = 0.2495E+01 : Gam_Z in GeV
EEM_H    = 0.3133E+00 : e = (4*pi*alpha_em)^1/2
ASMT_H   = 0.1084E+00 : alpha_s(M_t^pole)
CW_H     = 0.8768E+00 : cosTheta_W
TW_H     = 0.5483E+00 : tanTheta_W
MW_H     = 0.7996E+02 : W boson mass MW = MZ*CW
GW_H     = 0.6517E+00 : SU(2) gauge coupling  gw=e/s_W
GP_H     = 0.3573E+00 : U(1)_Y gauge coupling gp=e/c_W
V_H      = 0.2454E+03 : V = 2 MW / gw
GF_H     = 0.1174E-04 : GF=sqrt(2)*gw^2/8 MW^2 in GeV^-2
MTMT_H   = 0.1666E+03 : t-quark mass at M_t^pole in GeV
----------------------------------------------------------
CKM Matrix :
|V_ud|   = |(0.9738E+00 0.0000E+00)| = 0.9738E+00
|V_us|   = |(0.2272E+00 0.0000E+00)| = 0.2272E+00
|V_ub|   = |(0.2174E-02 -.3349E-02)| = 0.3993E-02
|V_cd|   = |(-.2271E+00 -.1377E-03)| = 0.2271E+00
|V_cs|   = |(0.9730E+00 -.3213E-04)| = 0.9730E+00
|V_cb|   = |(0.4222E-01 0.0000E+00)| = 0.4222E-01
|V_td|   = |(0.7478E-02 -.3259E-02)| = 0.8157E-02
|V_ts|   = |(-.4161E-01 -.7602E-03)| = 0.4162E-01
|V_tb|   = |(0.9991E+00 0.0000E+00)| = 0.9991E+00
----------------------------------------------------------
Real SUSY Parameters  in /HC_RSUSYPARA/
----------------------------------------------------------
TB_H     = 0.5000E+01 : tan(beta)
CB_H     = 0.1961E+00 : cos(beta)
SB_H     = 0.9806E+00 : sin(beta)
MQ3_H    = 0.5000E+03 : M_tildeQ_3 in GeV
MU3_H    = 0.5000E+03 : M_tildeU_3 in GeV
MD3_H    = 0.5000E+03 : M_tildeD_3 in GeV
```

```
 ML3_H    = 0.5000E+03 : M_tildeL_3 in GeV
 ME3_H    = 0.5000E+03 : M_tildeE_3 in GeV
---------------------------------------------------------
 Complex SUSY Parameters  in /HC_CSUSYPARA/
---------------------------------------------------------
 |MU_H|     = 0.2000E+04:Mag. of MU parameter in GeV
 |M1_H|     = 0.5000E+02:Mag. of M1 parameter in GeV
 |M2_H|     = 0.1000E+03:Mag. of M2 parameter in GeV
 |M3_H|     = 0.1000E+04:Mag. of M3 parameter in GeV
 |AT_H|     = 0.1000E+04:Mag. of AT parameter in GeV
 |AB_H|     = 0.1000E+04:Mag. of AB parameter in GeV
 |ATAU_H|   = 0.1000E+04:Mag. of ATAU parameter in GeV
 ARG(MU_H)  = 0.0000E+00:Arg. of MU parameter in Degree
 ARG(M1_H)  = 0.0000E+00:Arg. of M1 parameter in Degree
 ARG(M2_H)  = 0.0000E+00:Arg. of M2 parameter in Degree
 ARG(M3_H)  = 0.9000E+02:Arg. of M3 parameter in Degree
 ARG(AT_H)  = 0.9000E+02:Arg. of AT parameter in Degree
 ARG(AB_H)  = 0.9000E+02:Arg. of AB parameter in Degree
 ARG(ATAU_H)= 0.9000E+02:Arg. of ATAU parameter in Degree
---------------------------------------------------------
 Diagonal Sfermion Mass Matrices [GeV] (Not squared) :
 M_Q = 0.5000E+03 x Diag(0.1000E+01 0.1000E+01 0.1000E+01)
 M_U = 0.5000E+03 x Diag(0.1000E+01 0.1000E+01 0.1000E+01)
 M_D = 0.5000E+03 x Diag(0.1000E+01 0.1000E+01 0.1000E+01)
 M_L = 0.5000E+03 x Diag(0.1000E+01 0.1000E+01 0.1000E+01)
 M_E = 0.5000E+03 x Diag(0.1000E+01 0.1000E+01 0.1000E+01)
---------------------------------------------------------
 Charged Higgs boson pole mass : 0.3000E+03 GeV
---------------------------------------------------------
```

- `IFLAG_H(2)` $= 1$: The masses and mixing matrix of the neutral Higgs boson change due to the improvement in their calculations and the new input for the b-quark mass.

```
---------------------------------------------------------
 Masses and Mixing Matrix of Higgs bosons :
                              HMASS_H(I) and OMIX_H(A,I)
---------------------------------------------------------
 H1  Pole Mass           = 0.1193E+03 GeV
 H2  Pole Mass           = 0.2718E+03 GeV
 H3  Pole Mass           = 0.2983E+03 GeV
```

```
 Charged Higgs Pole Mass = 0.3000E+03 GeV [SSPARA_H(2)]
                         [H1]         [H2]         [H3]
           [phi_1] / 0.2457E+00  0.3360E+00  0.9093E+00  \
 O(IA,IH)= [phi_2] | 0.9693E+00  -.7551E-01  -.2340E+00  |
           [  a  ] \ -.9973E-02  0.9388E+00  -.3442E+00  /
---------------------------------------------------------
```

- IFLAG_H(14) $=1$: The elements of the propagator matrices $D^{H^0,H^\pm}(\hat{s})$ and the $\hat{s}$-dependent couplings of the neutral Higgs bosons to two photons, $S_i^\gamma(\sqrt{\hat{s}})$ and $P_i^\gamma(\sqrt{\hat{s}})$, and two gluons, $S_i^g(\sqrt{\hat{s}})$ and $P_i^g(\sqrt{\hat{s}})$, taking $\sqrt{\hat{s}}=M_{H_2}$. The couplings are compared to their values at the Higgs-boson pole masses: $S_i^\gamma(\sqrt{\hat{s}}=M_{\tt IH})=$ NHC_H(88, IH), $P_i^\gamma(\sqrt{\hat{s}}=M_{\tt IH})=$ NHC_H(89, IH), $S_i^g(\sqrt{\hat{s}}=M_{\tt IH})=$ NHC_H(84, IH), $P_i^g(\sqrt{\hat{s}}=M_{\tt IH})=$ NHC_H(85, IH).

```
---------------------------------------------------------
 DNH4 at sqrts = 0.2718E+03 GeV
---------------------------------------------------------
 DNH4[H1,H1]: |(0.1238E+01 0.2290E-01)| = 0.1238E+01
 DNH4[H2,H2]: |(0.5542E-01 -.1611E+04)| = 0.1611E+04
 DNH4[H3,H3]: |(-.4876E+01 -.2128E-01)| = 0.4876E+01
 DNH4[H1,H2]: |(-.1607E+00 -.2973E-02)| = 0.1608E+00
 DNH4[H1,H3]: |(-.5956E-05 0.2606E-03)| = 0.2606E-03
 DNH4[H2,H3]: |(-.4893E-01 -.2377E-03)| = 0.4893E-01
 DNH4[G0,H1]: |(0.3403E-06 -.1825E-04)| = 0.1825E-04
 DNH4[G0,H2]: |(0.1872E+00 0.2446E-05)| = 0.1872E+00
 DNH4[G0,H3]: |(-.2222E-06 0.5181E-04)| = 0.5182E-04
 DNH4[G0,G0]: |(0.1000E+01 -.2365E-05)| = 0.1000E+01
---------------------------------------------------------
 DCH2 at sqrts = 0.2718E+03 GeV
---------------------------------------------------------
 DCH2[H+,H+]: |(-.4576E+01 -.2790E-01)| = 0.4576E+01
 DCH2[H+,G+]: |(-.1256E-03 0.2294E-01)| = 0.2294E-01
 DCH2[G+,H+]: |(-.1256E-03 0.2294E-01)| = 0.2294E-01
 DCH2[G+,G+]: |(0.1000E+01 -.6202E-03)| = 0.1000E+01
---------------------------------------------------------
 Comparisons of the H-photon-photon couplings at MH^pole
 and those at sqrt{s} = 0.2718E+03 GeV
---------------------------------------------------------
                S couplings             P couplings
 H1PP(M): (-.6615E+01 0.6386E-01) (0.1303E-01 0.7314E-03)
```

```
 H1PP(S): (-.3180E+01 -.6078E+01) (0.1779E-01 0.2017E-02)
 H2PP(M): (-.9852E+00 0.3333E-01) (-.6867E+00 -.2221E+00)
 H2PP(S): (-.9852E+00 0.3333E-01) (-.6867E+00 -.2221E+00)
 H3PP(M): (-.4272E+00 0.2509E+00) (0.5178E+00 0.7028E-01)
 H3PP(S): (-.3695E+00 0.2852E+00) (0.4567E+00 0.7475E-01)
---------------------------------------------------------
 Comparisons of the H-glue-glue couplings at MH^pole
 and those at sqrt{s} = 0.2718E+03 GeV
---------------------------------------------------------
                S couplings            P couplings
 H1GG(M): (0.5792E+00 0.4164E-01) (0.5316E-02 -.6809E-03)
 H1GG(S): (0.7358E+00 0.8932E-02) (0.6510E-02 -.1457E-03)
 H2GG(M): (-.3557E+00 0.2591E-02) (-.1970E+00 -.3456E-01)
 H2GG(S): (-.3557E+00 0.2591E-02) (-.1970E+00 -.3456E-01)
 H3GG(M): (-.2240E+00 0.2860E-01) (0.1855E+00 0.2231E-02)
 H3GG(S): (-.2150E+00 0.3413E-01) (0.1585E+00 0.2662E-02)
---------------------------------------------------------
```

- `IFLAG_H(15)` = 1: The Higgs-mediated two-loop Thallium, electron, and muon EDMs. For the Thallium case, the two main contributions from the electron EDM and the CP-odd electron-nucleon interaction are shown separately.

```
---------------------------------------------------------
             Higgs-mediated two-loop EDMs
     Phi_3 = 0.9000E+02^o and Phi_At = 0.9000E+02^o
---------------------------------------------------------
 Thallium[10^-24 ecm]: -.2612E+01
                      [-.2568E+01 from electron EDM]
                      [-.4467E-01 from C_S      EDM]
 Electron[10^-26 ecm]: 0.4389E+00
 Muon[10^-24 ecm]    : 0.8997E+00
---------------------------------------------------------
```

- `IFLAG_H(16)` = 1: The B-meson observables.

```
---------------------------------------------------------
                     B Observables
---------------------------------------------------------
 B(B_s -> mu  mu )   x 10^7 = 0.3710E-01
 B(B   -> X_s gamma) x 10^4 = 0.4396E+01
 B(B_u -> tau nu)/B(SM)     = 0.9854E+00
```

```
 B(B_d -> tau tau)   x 10^7 = 0.2294E+00
 ACP(B -> X_s gamma) x 10^2 = -.7954E-01 [%]
 Delta M [B_d] (SUSY)       = 0.6659E-04 [1/ps]
 Delta M [B_s] (SUSY)       = 0.1982E-01 [1/ps]
---------------------------------------------------------
```

- `IFLAG_H(17)` = 1: The details of the $B \to X_s\gamma$ calculation. As a default, we use $m_c(\mu_c = m_c^{\rm pole})$ to capture a part of NNLO corrections [31]. The case when only the charged-Higgs contribution is added to the SM prediction is also shown.

```
---------------------------------------------------------
                    B -> X_s gamma
 delta and E_gamma^cut [GeV]: 0.3333E+00  0.1601E+01
---------------------------------------------------------
 b-q masses [GeV]  (pole,       @mb^pole,   @mt^pole):
                    0.4802E+01  0.4415E+01  0.3155E+01
 c-q masses [GeV]  (pole,       @mc^pole,   @mb^pole):
                    0.1415E+01  0.1250E+01  0.1029E+01
 mu_b and mu_c  [GeV]       : 0.4802E+01  0.1415+01
---------------------------------------------------------
 BR  x 10^4: 0.4396E+01 (SM+Charged Higgs+Chargino)
           [0.4471E+01 (SM+Charged Higgs)]
           [0.3351E+01 (SM)]
 ACP x 10^2: -.7954E-01 %
---------------------------------------------------------
```

References

[1] For a recent review, see T. Ibrahim and P. Nath, arXiv:0705.2008 [hep-ph].

[2] For reviews, see M. Trodden, in the *Proceedings of 32nd SLAC Summer Institute on Particle Physics (SSI 2004): Nature's Greatest Puzzles*, Menlo Park, California, 2-13 Aug 2004, pp L018 [arXiv:hep-ph/0411301]; M. Quiros, J. Phys. A **40** (2007) 6573; W. Buchmuller, arXiv:0710.5857 [hep-ph].

[3] J. S. Lee, A. Pilaftsis, M. Carena, S. Y. Choi, M. Drees, J. R. Ellis and C. E. M. Wagner, Comput. Phys. Commun. **156** (2004) 283 [arXiv:hep-ph/0307377].

[4] S. Heinemeyer, W. Hollik and G. Weiglein, *Comp. Phys. Comm.* **124** 2000 76, hep-ph/9812320; T. Hahn, S. Heinemeyer, W. Hollik, H. Rzehak and G. Weiglein, arXiv:0710.4891 [hep-ph].

[5] J. Ellis, J. S. Lee and A. Pilaftsis, arXiv:0708.2079 [hep-ph].

[6] M. Carena, J. R. Ellis, A. Pilaftsis and C. E. M. Wagner, Nucl. Phys. B **625** (2002) 345 [arXiv:hep-ph/0111245].

[7] M. Carena, J. R. Ellis, A. Pilaftsis and C. E. M. Wagner, Nucl. Phys. B **586** (2000) 92 [arXiv:hep-ph/0003180].

[8] M. Carena, J. R. Ellis, A. Pilaftsis and C. E. M. Wagner, Phys. Lett. B **495** (2000) 155 [arXiv:hep-ph/0009212].

[9] J. R. Ellis, J. S. Lee and A. Pilaftsis, Phys. Rev. D **70** (2004) 075010 [arXiv:hep-ph/0404167].

[10] A. Pilaftsis, Nucl. Phys. B **504** (1997) 61.

[11] J. M. Cornwall and J. Papavassiliou, Phys. Rev. D **40** (1989) 3474;
J. Papavassiliou, Phys. Rev. D **41** (1990) 3179;
D. Binosi and J. Papavassiliou, Phys. Rev. D **66** (2002) 111901; J. Phys. G **30** (2004) 203.

[12] J. R. Ellis, J. S. Lee and A. Pilaftsis, Nucl. Phys. B **718** (2005) 247 [arXiv:hep-ph/0411379]; J. S. Lee, Mod. Phys. Lett. A **22** (2007) 1191 [arXiv:0705.1089 [hep-ph]].

[13] J. Guasch, W. Hollik and S. Penaranda, Phys. Lett. B **515** (2001) 367 [arXiv:hep-ph/0106027].

[14] I.B. Khriplovich and S.K. Lamoreaux, *CP Violation Without Strangeness* (Springer, New York, 1997).

[15] For a recent review, see, M. Pospelov and A. Ritz, Annals Phys. **318** (2005) 119.

[16] For two-loop Higgs-mediated contributions to EDMs in the CP-violating MSSM, see D. Chang, W.-Y. Keung and A. Pilaftsis, Phys. Rev. Lett. **82** (1999) 900; A. Pilaftsis, Nucl. Phys. B **644** (2002) 263; D. A. Demir, O. Lebedev, K. A. Olive, M. Pospelov and A. Ritz, Nucl. Phys. B **680** (2004) 339; K. A. Olive, M. Pospelov, A. Ritz and Y. Santoso, Phys. Rev. D **72** (2005) 075001 [arXiv:hep-ph/0506106].

[17] J. R. Ellis, J. S. Lee and A. Pilaftsis, Phys. Rev. D **72** (2005) 095006 [arXiv:hep-ph/0507046].

[18] J. S. Lee and S. Scopel, Phys. Rev. D **75** (2007) 075001 [arXiv:hep-ph/0701221]; J. S. Lee, arXiv:0706.2222 [hep-ph].

[19] B. C. Regan, E. D. Commins, C. J. Schmidt and D. DeMille, Phys. Rev. Lett. **88** (2002) 071805.

[20] G. Abbiendi *et al.* [OPAL Collaboration], Eur. Phys. J. C **37** (2004) 49 [arXiv:hep-ex/0406057]; OPAL Physics Note PN505, `http://opal.web.cern.ch/Opal/pubs/physnote/html/pn505.html`; A. Heister *et al.* [ALEPH Collaboration], Phys. Lett. B **526** (2002) 191 [arXiv:hep-ex/0201014]; J. Abdallah *et al.* [DELPHI Collaboration], Eur. Phys. J. C **32** (2004) 145 [arXiv:hep-ex/0303013]; P. Achard *et al.* [L3 Collaboration], Phys. Lett. B **545** (2002) 30 [arXiv:hep-ex/0208042]; S. Schael *et al.* [ALEPH Collaboration], Eur. Phys. J. C **47** (2006) 547 [arXiv:hep-ex/0602042].

[21] P. Franzini *et al.*, Phys. Rev. D **35**, 2883 (1987).

[22] W. M. Yao *et al.* [Particle Data Group], J. Phys. G **33** (2006) 1.

[23] A. Dedes and A. Pilaftsis, Phys. Rev. D **67** (2003) 015012 [arXiv:hep-ph/0209306].

[24] C. Collaboration and T. Aaltonen, arXiv:0712.1708 [hep-ex].

[25] E. Barberio *et al.* [Heavy Flavor Averaging Group (HFAG) Collaboration], arXiv:0704.3575 [hep-ex].

[26] M. S. Carena, D. Garcia, U. Nierste and C. E. M. Wagner, Phys. Lett. B **499**, 141 (2001) [arXiv:hep-ph/0010003]. G. Degrassi, P. Gambino and G. F. Giudice, JHEP **0012**, 009 (2000) [arXiv:hep-ph/0009337].

[27] F. Borzumati, J. S. Lee and W. Y. Song, Phys. Lett. B **595** (2004) 347. [arXiv:hep-ph/0401024].

[28] K. Ikado *et al.*, Phys. Rev. Lett. **97** (2006) 251802. [arXiv:hep-ex/0604018]; B. Aubert [The BABAR Collaboration], arXiv:0708.2260 [hep-ex].

[29] B. Aubert *et al.* [BABAR Collaboration], Phys. Rev. Lett. **96** (2006) 241802 [arXiv:hep-ex/0511015].

[30] H. G. Evans [CDF Collaboration], arXiv:0705.4598 [hep-ex].

[31] M. Misiak *et al.*, Phys. Rev. Lett. **98** (2007) 022002, [arXiv:hep-ph/0609232].

Table 1: *The contents of the array* RAUX_H. *In* RAUX_H(22) *and* RAUX_H(23), *the notation* h^0_f *is for the Yukawa couplings without including the threshold corrections. The notations which are not explained in the text follow the conventions of* CPsuperH *[3] and Refs. [5–7].*

RAUX_H(1)	$m_b^{\rm pole}$	RAUX_H(26)	$\|h_t(Q_{tb})\|$	RAUX_H(120)	$d^H_\mu \times 10^{24}\, e\, cm$
RAUX_H(2)	$m_b(m_b^{\rm pole})$	RAUX_H(27)	$\|h_b(m_t^{\rm pole})\|$	...	...
RAUX_H(3)	$\alpha_s(m_b^{\rm pole})$	RAUX_H(28)	$\|h_b(Q_b)\|$	...	...
RAUX_H(4)	$m_c^{\rm pole}$	RAUX_H(29)	$\|h_b(Q_{tb})\|$	...	...
RAUX_H(5)	$m_c(m_c^{\rm pole})$	RAUX_H(30)	M_A^2	...	...
RAUX_H(6)	$\alpha_s(m_c^{\rm pole})$	RAUX_H(31)	$\Re{\rm e}\widehat{\Pi}_{H^+H^-}(M_{H^\pm}^{{\rm pole}\,2})$	...	...
...	...	RAUX_H(32)	$\bar\lambda_4 v^2(m_t^{\rm pole})/2$	...	...
...	...	RAUX_H(33)	$\bar\lambda_4(m_t^{\rm pole})$	RAUX_H(130)	$B(B_s\to\mu\mu)\times 10^7$
...	...	RAUX_H(34)	$\bar\lambda_1(m_t^{\rm pole})$	RAUX_H(131)	$B(B_d\to\tau\tau)\times 10^7$
RAUX_H(10)	$M_{H^\pm}^{\rm pole}$ or $M_{H^\pm}^{\rm eff.}$	RAUX_H(35)	$\bar\lambda_2(m_t^{\rm pole})$	RAUX_H(132)	$\Delta M_{B_d}^{\rm SUSY}$ ps^{-1}
RAUX_H(11)	Q_t^2	RAUX_H(36)	$\bar\lambda_{34}(m_t^{\rm pole})$	RAUX_H(133)	$\Delta M_{B_s}^{\rm SUSY}$ ps^{-1}
RAUX_H(12)	Q_b^2	...	...	RAUX_H(134)	$R_{B\tau\nu}$
RAUX_H(13)	Q_{tb}^2	...	...	RAUX_H(135)	$B(B\to X_s\gamma)\times 10^4$
RAUX_H(14)	$v_1(m_t^{\rm pole})$	RAUX_H(101)	$\sqrt{\hat s}$	RAUX_H(136)	$\mathcal{A}_{\rm CP}(B\to X_s\gamma)\,\%$
RAUX_H(15)	$v_1(Q_t)$	...	...	...	...
RAUX_H(16)	$v_1(Q_b)$	...	...	...	...
RAUX_H(17)	$v_1(Q_{tb})$	RAUX_H(111)	$d^H_{\rm Tl}\times 10^{24}\, e\, cm$	...	...
RAUX_H(18)	$v_2(m_t^{\rm pole})$	RAUX_H(112)	$(d^H_{\rm Tl})^{\,e}\times 10^{24}\, e\, cm$		
RAUX_H(19)	$v_2(Q_t)$	RAUX_H(113)	$(d^H_{\rm Tl})^{C_S}\times 10^{24}\, e\, cm$		
RAUX_H(20)	$v_2(Q_b)$	RAUX_H(114)	$d^H_e\times 10^{26}\, e\, cm$		
RAUX_H(21)	$v_2(Q_{tb})$	RAUX_H(115)	$(d^H_e)^{\tilde t}\times 10^{26}\, e\, cm$		
RAUX_H(22)	$\|h_t^0(m_t^{\rm pole})\|$	RAUX_H(116)	$(d^H_e)^{\tilde b}\times 10^{26}\, e\, cm$		
RAUX_H(23)	$\|h_b^0(m_t^{\rm pole})\|$	RAUX_H(117)	$(d^H_e)^{t}\times 10^{26}\, e\, cm$		
RAUX_H(24)	$\|h_t(m_t^{\rm pole})\|$	RAUX_H(118)	$(d^H_e)^{b}\times 10^{26}\, e\, cm$		
RAUX_H(25)	$\|h_t(Q_t)\|$	RAUX_H(119)	$(d^H_e)^{\tilde\chi^\pm}\times 10^{26}\, e\, cm$		

Table 2: *The contents of the array* `CAUX_H`. *The notations which are not explained in the text follow the* `CPsuperH` *[3] convention.*

`CAUX_H(1)`	$h_t/\lvert h_t\rvert$	`CAUX_H(112)`	$D^{H^0}_{4,1}(\hat{s})$	`CAUX_H(140)`	$S^g_1(\sqrt{\hat{s}})$
`CAUX_H(2)`	$h_b/\lvert h_b\rvert$	`CAUX_H(113)`	$D^{H^0}_{4,2}(\hat{s})$	`CAUX_H(141)`	$P^g_1(\sqrt{\hat{s}})$
...	...	`CAUX_H(114)`	$D^{H^0}_{4,3}(\hat{s})$	`CAUX_H(142)`	$S^g_2(\sqrt{\hat{s}})$
...	...	`CAUX_H(115)`	$D^{H^0}_{4,4}(\hat{s})$	`CAUX_H(143)`	$P^g_2(\sqrt{\hat{s}})$
...	...	`CAUX_H(116)`	$D^{H^\pm}_{H^\pm,H^\pm}(\hat{s})$	`CAUX_H(144)`	$S^g_3(\sqrt{\hat{s}})$
...	...	`CAUX_H(117)`	$D^{H^\pm}_{H^\pm,G^\pm}(\hat{s})$	`CAUX_H(145)`	$P^g_3(\sqrt{\hat{s}})$
`CAUX_H(100)`	$D^{H^0}_{1,1}(\hat{s})$	`CAUX_H(118)`	$D^{H^\pm}_{G^\pm,H^\pm}(\hat{s})$	...	...
`CAUX_H(101)`	$D^{H^0}_{1,2}(\hat{s})$	`CAUX_H(119)`	$D^{H^\pm}_{G^\pm,G^\pm}(\hat{s})$	...	...
`CAUX_H(102)`	$D^{H^0}_{1,3}(\hat{s})$	...	...	`CAUX_H(150)`	$\langle\bar{B}^0_d\rvert\, H^{\Delta B=2}_{\rm eff}\,\lvert B^0_d\rangle_{\rm SUSY}$
`CAUX_H(103)`	$D^{H^0}_{1,4}(\hat{s})$	...	...	`CAUX_H(151)`	$\langle\bar{B}^0_s\rvert\, H^{\Delta B=2}_{\rm eff}\,\lvert B^0_s\rangle_{\rm SUSY}$
`CAUX_H(104)`	$D^{H^0}_{2,1}(\hat{s})$	...	...	...	...
`CAUX_H(105)`	$D^{H^0}_{2,2}(\hat{s})$	`CAUX_H(130)`	$S^\gamma_1(\sqrt{\hat{s}})$	...	...
`CAUX_H(106)`	$D^{H^0}_{2,3}(\hat{s})$	`CAUX_H(131)`	$P^\gamma_1(\sqrt{\hat{s}})$	...	...
`CAUX_H(107)`	$D^{H^0}_{2,4}(\hat{s})$	`CAUX_H(132)`	$S^\gamma_2(\sqrt{\hat{s}})$	...	...
`CAUX_H(108)`	$D^{H^0}_{3,1}(\hat{s})$	`CAUX_H(133)`	$P^\gamma_2(\sqrt{\hat{s}})$	...	...
`CAUX_H(109)`	$D^{H^0}_{3,2}(\hat{s})$	`CAUX_H(134)`	$S^\gamma_3(\sqrt{\hat{s}})$	...	...
`CAUX_H(110)`	$D^{H^0}_{3,3}(\hat{s})$	`CAUX_H(135)`	$P^\gamma_3(\sqrt{\hat{s}})$	...	...
`CAUX_H(111)`	$D^{H^0}_{3,4}(\hat{s})$	...	...	...	...

Table 3: *The contents of the extended* `SMPARA_H(IP)`.

`IP`	Parameter	`IP`	Parameter	`IP`	Parameter	`IP`	Parameter
1	$\alpha^{-1}_{\rm em}(M_Z)$	6	m_μ	11	$m_u(m_t^{\rm pole})$	16	λ
2	$\alpha_s(M_Z)$	7	m_τ	12	$m_c(m_t^{\rm pole})$	17	A
3	M_Z	8	$m_d(m_t^{\rm pole})$	13	$m_t^{\rm pole}$	18	$\bar{\rho}$
4	$\sin^2\theta_W$	9	$m_s(m_t^{\rm pole})$	14	Γ_W	19	$\bar{\eta}$
5	m_e	10	$m_b(m_t^{\rm pole})$	15	Γ_Z	20	...

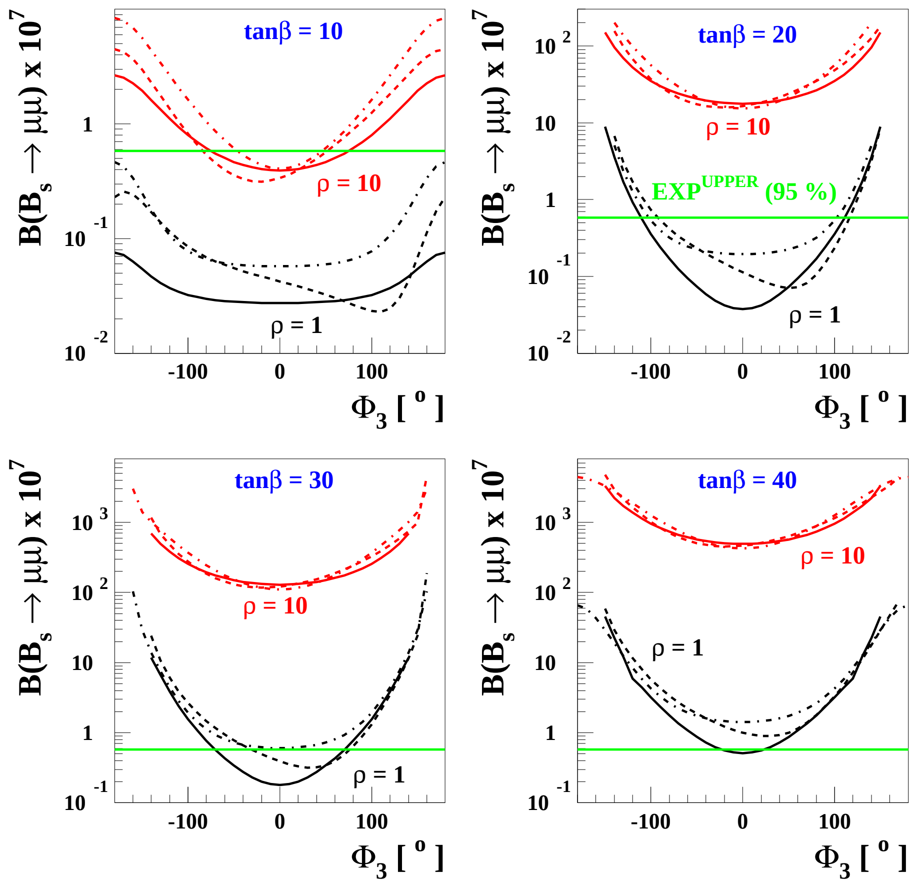

Figure 5: *The branching ratio* $B(B_s \to \mu^+\mu^-) \times 10^7$ *as a function of* Φ_3 *for four values of* $\tan\beta$*:* $\tan\beta = 10$ *(upper left), 20 (upper right), 30 (lower left), and 40 (lower right). The CPX scenario is taken with* $M_{\rm SUSY} = 0.5$ *TeV and* $M_{H^\pm} = 200$ *GeV in the convention* $\Phi_\mu = 0$*. In each frame, the lower three lines are for the case* $\rho \equiv \rho_{\tilde{Q}} = \rho_{\tilde{U}} = \rho_{\tilde{D}} = 1$ *and the upper lines for* $\rho = 10$ *where the solid, dashed, and dash-dotted lines are for* $\Phi_A = 0°$*,* $90°$*, and* $180°$*, respectively. The current 95 % experimental upper bound,* 5.8×10^{-8} *[24], is also shown as a horizontal line in each frame.*

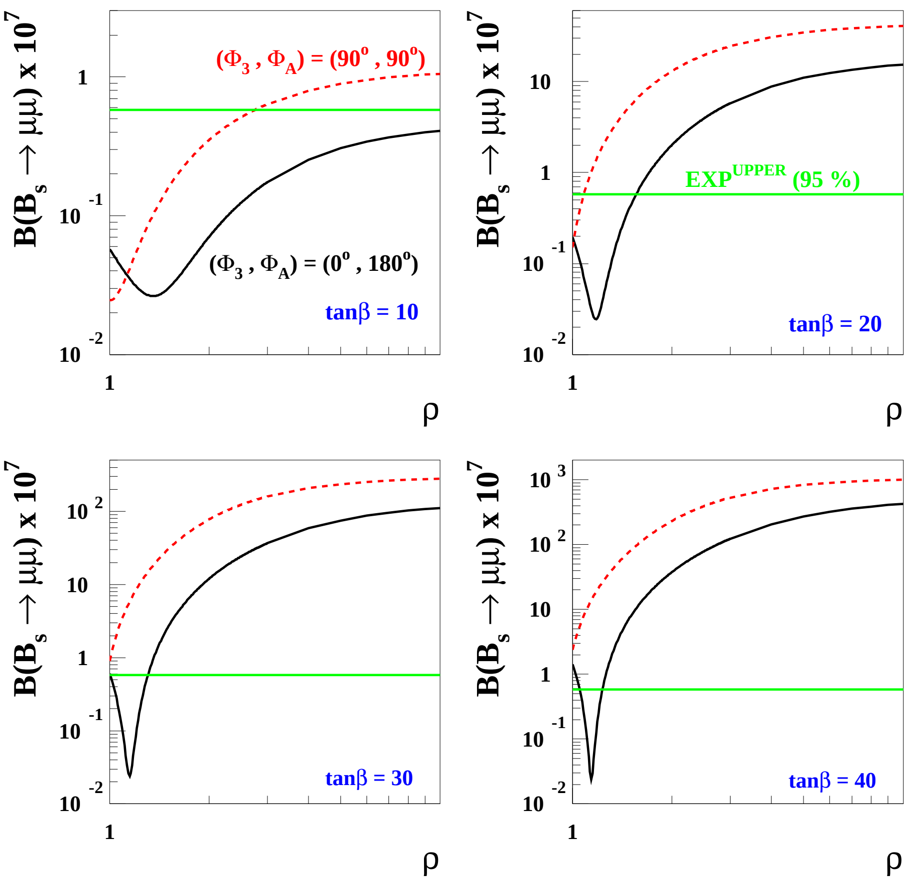

Figure 6: *The branching ratio* $B(B_s \to \mu^+\mu^-) \times 10^7$ *as a function of the common hierarchy factor* $\rho \equiv \rho_{\tilde{Q}} = \rho_{\tilde{U}} = \rho_{\tilde{D}}$ *for four values of* $\tan\beta$*:* $\tan\beta = 10$ *(upper left), 20 (upper right), 30, (lower left), and 40 (lower right). The CPX scenario is taken with* $M_{\rm SUSY} = 0.5$ *TeV and* $M_{H^\pm} = 200$ *GeV in the convention* $\Phi_\mu = 0$*. In each frame, the solid line is for* $(\Phi_3\,,\Phi_A) = (0^\circ\,,180^\circ)$ *and the dashed one for* $(90^\circ\,,90^\circ)$*. The current 95 % experimental upper bound,* 5.8×10^{-8} *[24], is also shown as a horizontal line in each frame.*

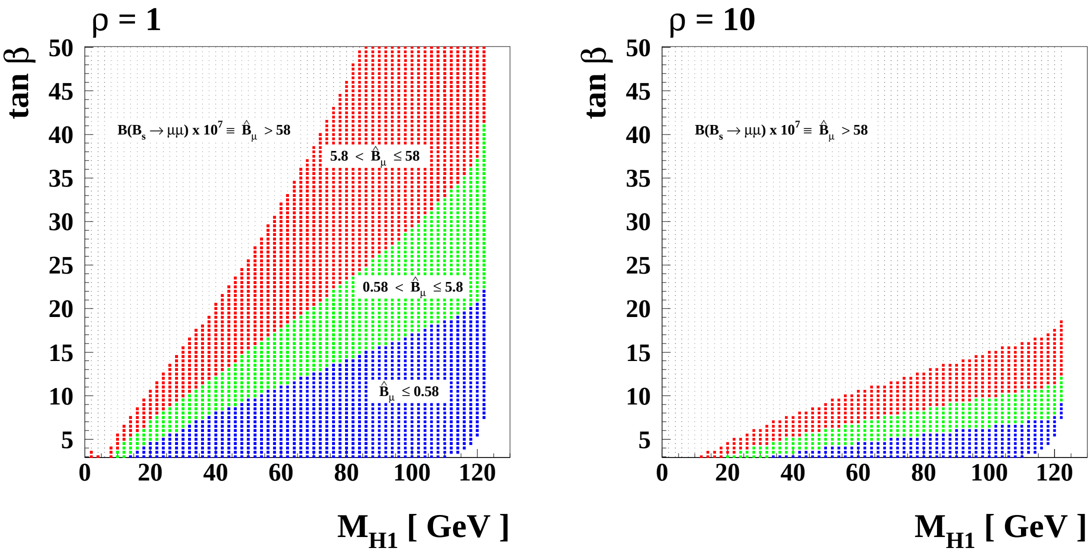

Figure 7: *The branching ratio* $\widehat{B}_\mu \equiv B(B_s \to \mu^+\mu^-) \times 10^7$ *in the* $(\tan\beta\,, M_{H_1})$ *plane. The CPX scenario is taken with* $\Phi_A = \Phi_3 = 90^\circ$ *and* $M_{\rm SUSY} = 0.5$ *TeV for two values of the common hierarchy factor:* $\rho = 1$ *(left) and* 10 *(right). The unshaded region is not theoretically allowed. The different shaded regions correspond to different ranges of* $\widehat{B}_\mu$*, as shown: specifically,* $\widehat{B}_\mu < 0.58$ *in the lowest (blue) low-*$\tan\beta$ *region, consistent with the current upper limit at 95 % C.L.*

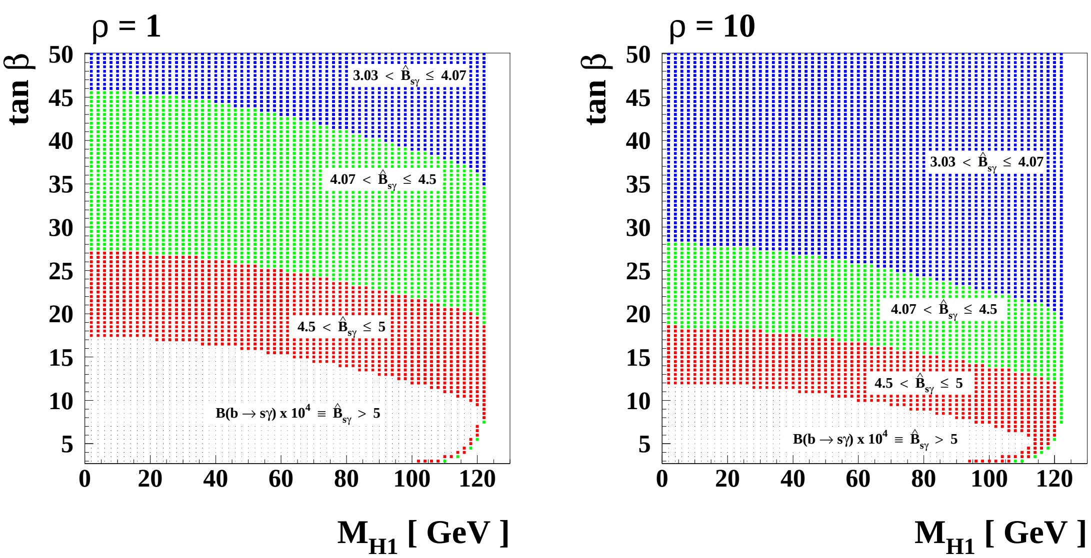

Figure 8: *The branching ratio* $\widehat{B}_{s\gamma} \equiv B(B \to X_s\gamma) \times 10^4$ *in the* $(\tan\beta\,, M_{H_1})$ *plane. The same CPX scenario with* $\Phi_A = \Phi_3 = 90^\circ$ *is taken as in Fig. 7. The different shaded regions correspond to different ranges of* $\widehat{B}_{s\gamma}$*, as shown: specifically,* $3.03 < \widehat{B}_{s\gamma} \leq 4.07$ *in the upmost (blue) high-tan*β *region, consistent with the current experimentally allowed 2-*σ *region,* $3.03 < \widehat{B}_{s\gamma} \leq 4.07$ *[25].*

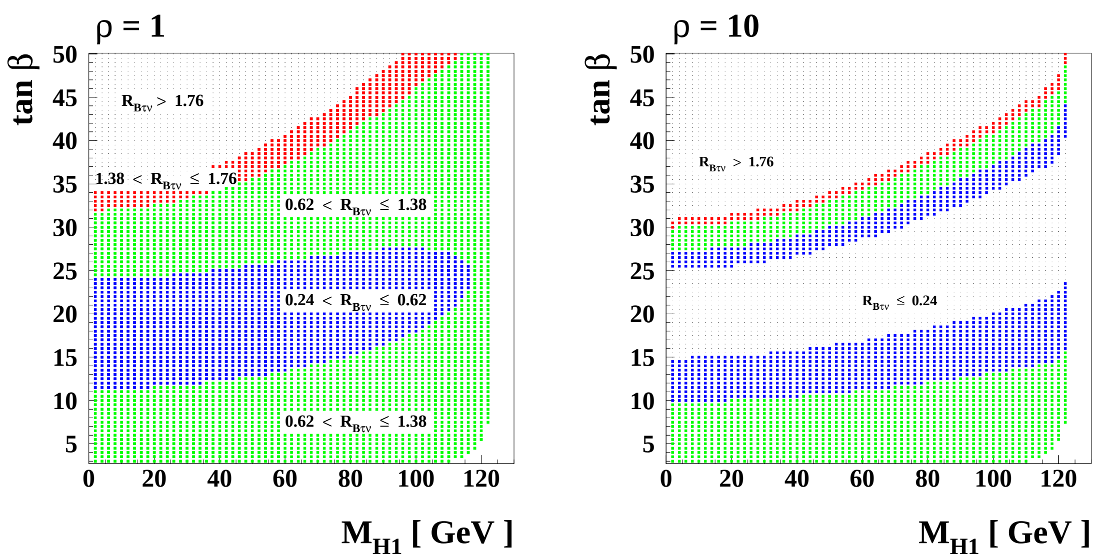

Figure 9: *The ratio* $R_{B\tau\nu}$ *in the* $(\tan\beta\,, M_{H_1})$ *plane. The same CPX scenario with* $\Phi_A = \Phi_3 = 90^\circ$ *is taken as in Fig. 7 for two values of* ρ*:* $\rho = 1$ *(left) and* 10 *(right). The different shaded regions correspond to the regions allowed at the 1-*σ *and 2-*σ *levels by the recent BELLE and BABAR results:* $R^{\rm EXP}_{B\tau\nu} = 1.0 \pm 0.38$ *[5, 28]. In the right frame, specifically, the 2-*σ *excluded regions are shown as* $R_{B\tau\nu} > 1.76$ *(in the high-*$\tan\beta$ *region) and* $R_{B\tau\nu} \le 0.24$ *(in the middle-*$\tan\beta$ *region).*

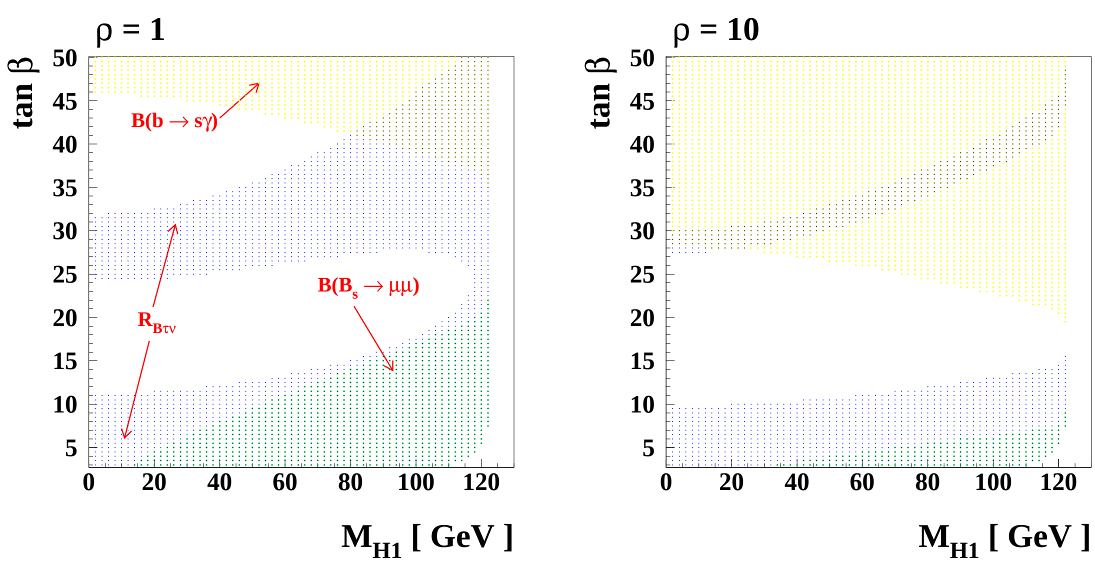

Figure 10: *The experimental constraints from* $B(B_s \to \mu^+\mu^-)$ *(95 %),* $B(B \to X_s\gamma)$ *(2* σ*), and* $R_{B\tau\nu}$ *(1* σ*) in the* $(\tan\beta\,, M_{H_1})$ *plane for two values of* ρ*. The same CPX scenario with* $\Phi_A = \Phi_3 = 90^\circ$ *is taken as in Fig. 7.*

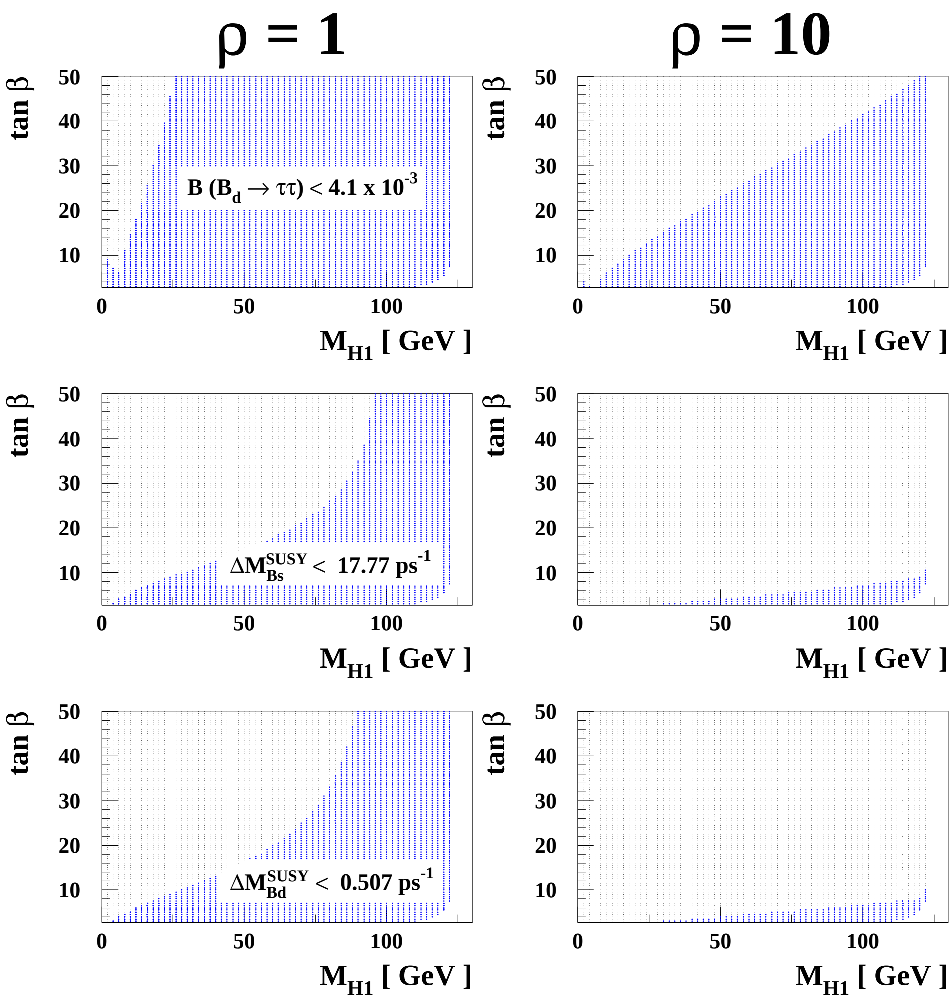

Figure 11: *The region allowed experimentally by the measurement* $B(B_d \to \tau^+\tau^-) < 4.1 \times 10^{-3}$ *(90 %) [29] (upper frames) and the regions where the SUSY contribution is smaller than the measured values of* B_s^0*-*$\bar{B}_s^0$ *mass difference [30] (middle frames) and* B_d^0*-*$\bar{B}_d^0$ *mass difference [22] (lower frames), in the* $(\tan\beta\,, M_{H_1})$ *plane. The left three frames are for* $\rho = 1$ *and the right ones for* $\rho = 10$*. The same CPX scenario with* $\Phi_A = \Phi_3 = 90^\circ$ *is taken as in Fig. 7.*

Table 4: *The contents of the extended* `SSPARA_H(IP)`.

`IP`	Parameter	`IP`	Parameter	`IP`	Parameter	`IP`	Parameter
1	$\tan\beta$	8	Φ_2	15	$m_{\tilde{E}_3}$	22	$\rho_{\tilde{Q}}$
2	$M_{H^\pm}^{\rm pole}$	9	$\|M_3\|$	16	$\|A_t\|$	23	$\rho_{\tilde{U}}$
3	$\|\mu\|$	10	Φ_3	17	Φ_{A_t}	24	$\rho_{\tilde{D}}$
4	Φ_μ	11	$m_{\tilde{Q}_3}$	18	$\|A_b\|$	25	$\rho_{\tilde{L}}$
5	$\|M_1\|$	12	$m_{\tilde{U}_3}$	19	Φ_{A_b}	26	$\rho_{\tilde{E}}$
6	Φ_1	13	$m_{\tilde{D}_3}$	20	$\|A_\tau\|$	27	...
7	$\|M_2\|$	14	$m_{\tilde{L}_3}$	21	Φ_{A_τ}	28	...